3

Cellular properties of principal neurons in the rat entorhinal cortex. II. The medial entorhinal cortex

Cathrin B. Canto [1, 2] and Menno P. Witter [1, 2]

[1] Kavli Institute for Systems Neuroscience and Centre for the Biology of Memory, Norwegian University of Science and Technology, NTNU, 7491 Trondheim, Norway

[2] VU University Medical Center, Department of Anatomy and Neurosciences, 1081 BT Amsterdam, The Netherlands

Under review at Hippocampus

3

Abstract

Principal neurons in different medial entorhinal cortex (MEC) layers show variations in spatial modulation, and the individual properties of neurons apparently stabilize between 15 and 30 days postnatally. The reported *in vivo* variations are likely due to differences in intrinsic membrane properties and integrative capacities of neurons. The latter depends on inputs and thus potentially on the morphology of principal neurons. In this comprehensive study, we systematically compared the morphological and physiological characteristics of principal neurons in all MEC layers. We recorded simultaneously from up to four post-hoc morphologically identified MEC principal neurons *in vitro.* Neurons in **L**(ayer) I-**L**III have dendritic and axonal arbors mainly in superficial layers, and **L**VI neurons mainly in deep layers. The dendritic and axonal trees of part of **L**V neurons diverge throughout all layers. Physiological properties of principal neurons differ between layers. In **L**II, most neurons have a prominent sag potential, resonance and membrane oscillations. Neurons in **L**III and **L**VI fire relatively regular, and lack sag potentials and membrane oscillations. **L**V neurons show the most prominent spike-frequency adaptation and highest input resistance. The data indicate that adult-like principal neuron types can be differentiated early on during postnatal development. The results of the accompanying paper, studying neurons in the lateral entorhinal cortex (LEC) [1], revealed that significant differences between LEC and MEC exist mainly in **L**II neurons. We therefore systematically analyzed changes in **L**II biophysical properties along the mediolateral axis of MEC and LEC. There is a systematic gradient in properties typical for MEC **L**II neurons. These properties are most pronounced in medially located neurons and become less apparent in more laterally positioned ones. This gradient continues into LEC, such that in LEC medially positioned neurons share some properties with adjacent MEC cells.

3 Introduction

The medial entorhinal cortex (MEC) has strong reciprocal connections with the hippocampus and plays a major role in memory processes [2-5]. In the rat, extracellular *in vivo* single unit recordings in MEC revealed that individual neurons are spatially modulated and contribute to spatial navigation and memory [3, 6-10]. Within MEC there is a functional differentiation between cell layers. Layer II (**L**II) contains mainly neurons that convey information about position and borders, called grid and border cells respectively, whereas layer III (**L**III), layer V (**L**V) and layer VI (**L**VI) neurons code additionally for direction (head direction cells) or a combination of the previous (conjunctive cells; [9, 10]). The intrinsic wiring and biophysical membrane properties of MEC neurons have been proposed as relevant factors for the layer specific differences in spatial coding, and more in particular the emergence of grid cell properties[11, 15].

Data on biophysical properties are available for some neurons in MEC. In particular properties of **L**II neurons have been studied extensively [12, 15-18]. Data are more sparse for neurons in **L**III and **L**V [18-25]. For neurons in layer I (**L**I) and **L**VI data are not available and as yet, there has been no systematic study of neurons in all layers of MEC using standardized experimental approaches. We engaged in a comprehensive survey of all types of principal neurons in both subdivisions of EC, using standardized conditions. In view of ongoing studies addressing the maturation of spatially modulated neurons in MEC [26, 27] it is important to establish which cell types are present in younger animals. We therefore aimed to describe the principal neuron types in young animals ranging from postnatal day 14 (P14) to P32. We report data obtained by performing up to four simultaneous whole cell current-clamp recordings from post-hoc morphologically identified principal neurons in all MEC layers to define layer specific physiological membrane properties. Morphologically, MEC principal neurons showed layer specific distributions of their dendritic and axonal tree, as well as layer specific physiological properties. In case of **L**II, morphologically different neurons also show differences in their overall electrophysiological profile. Such clear relations between morphology and electrophysiology are not apparent for neurons in any of the remaining layers. Moreover the combined data obtained in this study when compared to published data on young adult animals, leads us to conclude that all major neuron types are already present in young postnatal animals.

This paper is the counterpart of a paper on neuronal properties in the lateral entorhinal cortex (LEC: [1]). The experimental procedures used to obtain both datasets were the same, truly allowing for the comparison of morphological and electrophysiological properties of neurons in both entorhinal subdivisions. We conclude that since the majority of these properties in **L**III-**L**VI of LEC and

MEC are similar, the overall differences in *in vivo* properties of both entorhinal subdivisions [28, 29] are not solely dependent on intrinsic principal neurons properties in **L**III-**L**VI. Neurons in **L**II are the exception. Prominent differences in physiological properties exist between MEC and LEC **L**II neurons, though no sharp transition at the border between the two parts was observed. The latter observation indicates that entorhinal **L**II neurons may rather have gradient-like distributed properties reminiscent of the entorhinal bands defined on the basis of topographically organized hippocampal connections [30-33] and intrinsic connections [34].

3.1 Methods

Animal experiments were performed in accordance with the rules and directives set by the Norwegian Government, the Norwegian University of Science and Technology (NTNU) and the European Community on animal well-being.

Slice preparation. Ninety juvenile Sprague Dawley rats between the age of P14 and P31 were anaesthetized with isofluorane (Isofane, Vercore, Marlow, UK) and subsequently decapitated. After opening the skull, the hemispheres were separated, the frontal part and the cerebellum removed, the hemispheres removed from the skull, and placed in ice-cold artificial cerebrospinal fluid (ACSF) for up to four minutes, saturated with 95 % O_2 / 5 % CO_2. The ACSF contained (mM): 126 NaCl, 3 KCl, 1.25 NaH_2PO_4, 2 $MgSO_4$, 2 $CaCl_2$, 10 Glucose, 26 $NaHCO_3$. After that 400 µm thick horizontal entorhinal slices were cut in ice-cold ACSF (Fig. 1). The slices were transferred into a holding chamber with oxygenated ACSF at room temperature and stored for at least one hour until used one by one in the recording chamber. All recordings were performed as described in detail in the accompanying paper [1], to which the reader is referred. Details on data analyses and histological procedures can also be found there. We ensured to systematically obtain slices in all animals at corresponding dorsal to ventral levels (Fig. 1) in order to increase the specificity of the obtained data. We recorded from 266 neurons in MEC: 109 X one neuron/slice, 48 X two neurons/slice, 13 X three neurons/slice, four X four neurons/slice and once six neurons/slice (Table 1).

No. neurons per slice / layer patched	1	2	3	4	5	6
LI	8					
LII	23	13	6	3		1
LIII	33	10	2			
LV	37	9	1	1		
LVI	8	3				
LII & LIII		7				
LIII & LV		5				
LII & LV		1				
LII & 2 LIII			1			
LIII & 2 LV			1			
LII & LIII & LV			2			

Table 1: Number of times a particular combination of MEC principal neurons was patched simultaneously, grouped according to layers. Rows indicate the MEC layer(s) the soma(ta) of neuron(s) resided in and columns the number neurons patched simultaneously. In each slice indicated, all neurons were patched synchronously except for the last column where we patched 6 **L**II neurons in two series one series of four and one of two.

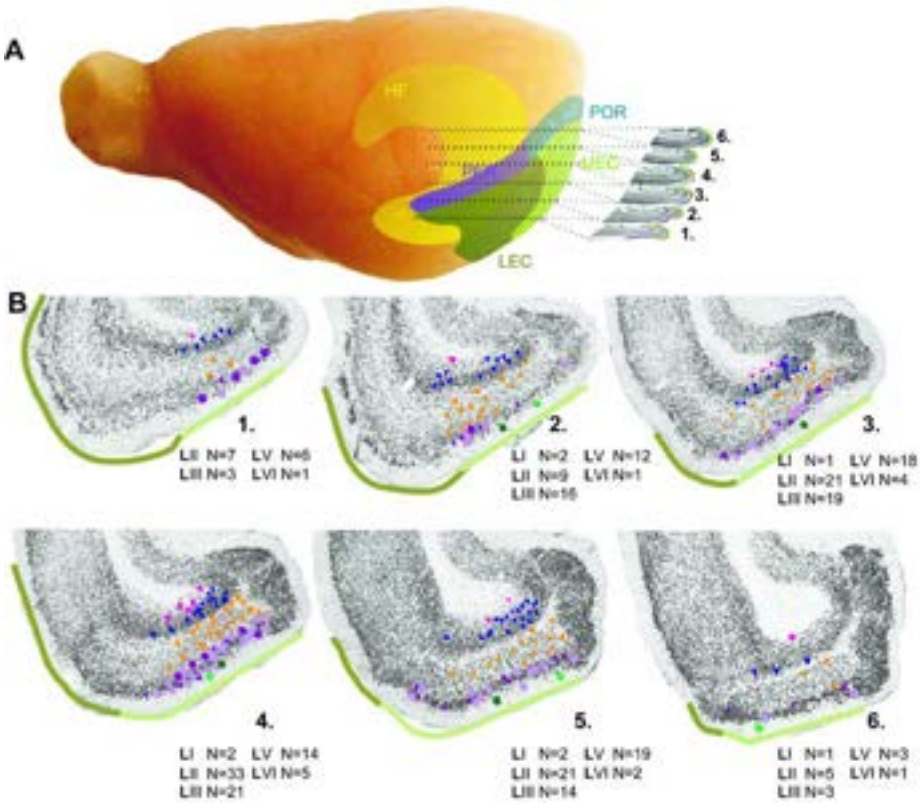

Figure 1: Schematic representation of the recording positions in MEC. **(A)** Schematic representation showing the location of the parahippocampal region and its different constituents: MEC (light green), LEC (dark green), the perirhinal cortex (PER, light purple), postrhinal cortex (POR, light blue), as well as the position of the hippocampal formation (HF, yellow) in the left hemisphere of a rat brain. The dorsoventral positions of the six used horizontal slices are shown. In corresponding Nissl-stained sections the extent of the different components of the parahippocampal region is color-coded **(B)** Location of examined MEC neurons along the mediolateral and dorsoventral axes. (1-6) High power photomicrographs of horizontal sections organized from ventral till dorsal illustrating the position and type of recorded neurons in different layers. Symbols represent different morphological groups and colors different layers. **L**I principal neurons without oscillations are green, with oscillations light green, **L**II principal neurons without oscillations are purple, with oscillations light purple. **L**III neurons are orange, **L**V blue and **L**VI principal neurons pink. Multipolar neurons are indicated by circles, and pyramidal or oblique pyramidal neurons as triangles or tilted triangles. Neurons in **L**II with a SC morphology are indicated by pentagons.

Statistical data analysis. All values presented in figures or in the text are either single data values of a representative neuron or means ± standard error of the mean (s.e.m.). A statistical comparison between groups was either performed

with repeated measures analysis, univariate (ANOVA) or multivariate analysis of variance (MANOVA) followed by post-hoc Bonferroni tests and Levene's tests to check for homogeneity of variance. When the assumptions for a parametric test were not met Kruskal-Wallis followed by Mann-Whitney U tests with a Bonferroni correction were performed. Results were considered significant at $p < 0.05$ for the parametric tests and $p < 0.01$ for the non-parametric tests. To analyze whether a mediolateral gradient in properties of **L**II neurons existed, we performed a linear regression analysis.

3.2 Results

We recorded from a total of 266 putative principal neurons in all layers of MEC, covering most of the dorsoventral and mediolateral extents: eight **L**I, 96 **L**II, 76 **L**III, 72 **L**V and 14 anatomically and physiologically identified **L**VI MEC putative principal neurons from 60 rats (Fig. 1).

Layer I

Morphological properties.

We recorded from principal neurons in deep **L**I of MEC. All **L**I principal neurons have big cell bodies with a diameter of >15 µm. Four to eight non–spiny apical dendrites branch shortly after leaving the soma and radiate within **L**I up to the pia. We observed two morphological types of neurons, horizontal and multipolar ones. Horizontal neurons have non-spiny dendrites that run largely parallel to the pial surface (Fig. 2A; N=4), whereas the non-spiny to sparsely spiny dendrites of multipolar neurons distribute in various directions (Fig. 2A; N=4). The two neuron types also differ regarding their dendritic spread. The horizontal dendritic spread of horizontal neurons can be up to 700 µm, whereas that of multipolar neurons is up to 600 µm (Fig. 2B). The basal dendrites of both neuron types extend into superficial **L**II (N=7). We were always able to follow the axons of horizontal and multipolar neurons into **L**III, whereas in two cases we could follow the axon until the angular bundle.

Electrophysiological properties.

The physiological responses of all described neurons allowed characterizing them as principal neurons (Fig. 2C). **L**I principal neurons have a lower input resistance than **L**III-**L**VI principal neurons but this is only significant compared to **L**V ones (Fig. 3A).

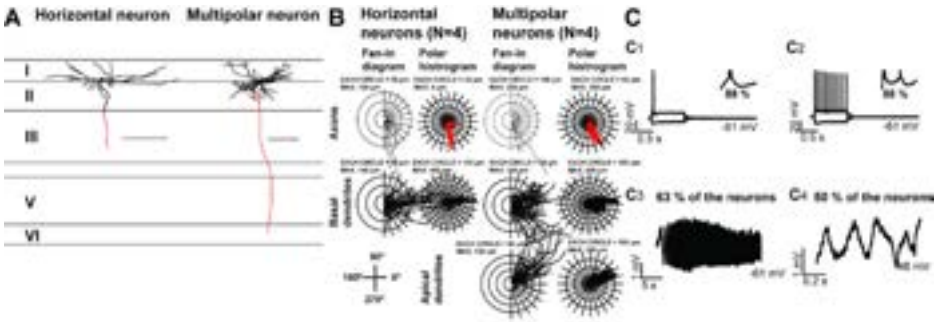

Figure 2: Morphology and physiology of MEC **L**I principal neurons. **(A)** Camera lucida drawings of one representative horizontal (left) and one multipolar (right) **L**I principal neuron. Horizontal lines indicate borders between layers of MEC. Dendrites are represented in black and axons in red. Scale bars: 200 µm. **(B)** Morphological properties. Fan-in diagrams (left) and corresponding polar histogram plots (right) for each morphological subtype of the axons (top), basal dendrites (middle), and apical dendrites (bottom). The number of neurons (N=) is indicated. Note that the histograms of both subtypes look rather similar except that horizontal neurons do not have basal dendrites. **(C)** **L**I neurons have a big sag potential, rebound and DAP amplitude together with marked resonance properties and membrane potential oscillations. **C**$_1$. Voltage responses of one typical **L**I neuron to a weak hyperpolarizing and depolarizing 1 s current step just reaching firing threshold. **C**$_2$.The voltage responses to a ±200 pA step of 1 s. **C**$_1$ and **C**$_2$. Insets show a zoom in of 20 ms, displaying the AP afterpotentials of the same neuron. Below insets the percentages of neurons with a DAP are listed. **C**$_3$. An example of a voltage response to a ZAP stimulus as seen in 63 percent of the recorded neurons. **C**$_4$. Membrane potential oscillations just below firing threshold, as recorded in 50 percent of the neurons. In all subfigures the average membrane potential is indicated right below the individual voltage traces.

The time constant (tau) is significantly longer in **L**I compared to **L**II principal neurons but significantly shorter than in **L**III principal neurons (Fig. 3B). In addition **L**I principal neurons have a significantly lower sag ratio (100 percent have a sag ratio < 0.8 and 63 percent < 0.7; Fig. 3C), bigger rebound (Fig. 3D) and depolarizing afterpotential (DAP) amplitudes after action potentials (APs; Figs. 3E, 3F, and 2C$_{1, 2}$ insets) compared to **L**III-**L**VI principal neurons. **L**I principal neurons also have a sag potential in the depolarizing direction, which leads to strong depolarization at the beginning of a current step, which in turn induces early firing in response to weak current injection (Fig. 2C$_1$). Positive 200 pA injection leads in 87 percent of the neurons to bursting activity at the beginning of the step followed by regular firing (Figs. 2C$_2$, 4A$_1$, and 4B$_1$). The amplitude of APs does not decrease significantly in response to +200 pA depolarization (Fig. 4C$_1$). The mean rise time of the first AP is similar to the mean rise times of APs in principal neurons of other layers (Fig. 3G). The AP half-width is smaller than that of **L**V and **L**VI principal neurons (Fig. 3H).

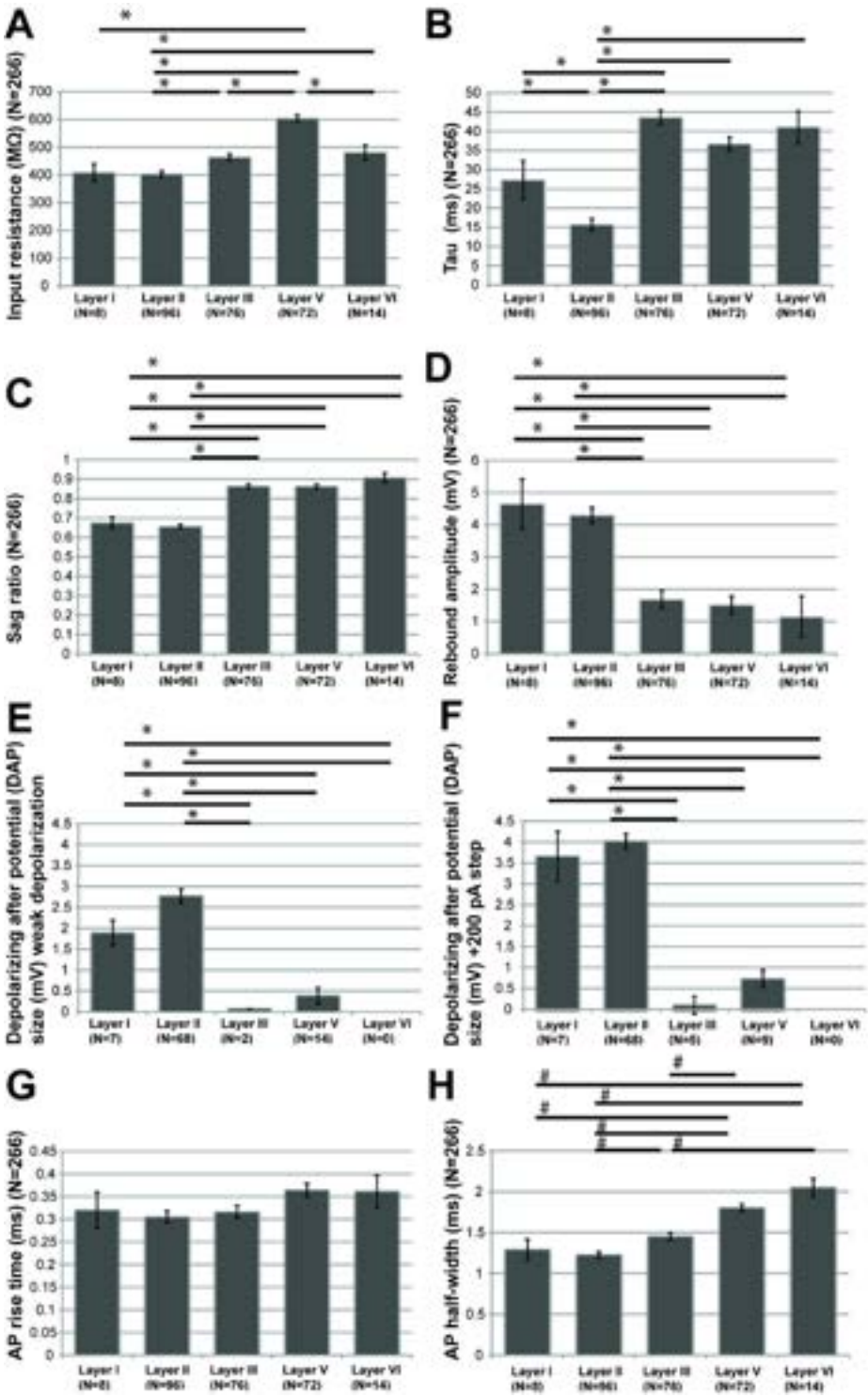
A
Input resistance (MΩ) (N=266)
B
Tau (ms) (N=266)
C
Sag ratio (N=266)
D
Rebound amplitude (mV) (N=266)
E
Depolarizing after potential (DAP) size (mV) weak depolarization
F
Depolarizing after potential (DAP) size (mV) +200 pA step
G
AP rise time (ms) (N=266)
H
AP half-width (ms) (N=266)
Layer I (N=8)
Layer II (N=96)
Layer III (N=76)
Layer V (N=72)
Layer VI (N=14)
Layer I (N=7)
Layer II (N=68)
Layer III (N=2)
Layer V (N=54)
Layer VI (N=0)
Layer III (N=5)
Layer V (N=9)

Figure 3: Summary histograms of physiological properties of principal neurons in all MEC layers. Data are averages with the error bars indicating s.e.m.. Significance is indicated with * if Kruskal-Wallis followed by Mann-Whitney U tests were performed with $p < 0.004$, # if (M)ANOVA followed by post-hoc Bonferroni tests were performed with $p < 0.05$. Number of neurons per layer is indicated with (N=). On the y-axis, the parameter measured is indicated and the total number of neurons in which this parameter was measured (N=). **(A)** Input resistance. **L**V neurons have a significantly higher input resistance compared to neurons in all other layers. Input resistance is measured by dividing the amplitude of the voltage response with that of the current step injected. **(B)** The time constant (tau) differs significantly between layers, with principal neurons in all layers having a longer time constant compared to **L**II. Time constant is defined as the time for the voltage deflection to reach 63 percent of its maximal value in response to a negative current step. We measured it for the step that lead to a steady state voltage deflection between -70 and -75 mV. **(C)** The sag ratio is significantly lower for principal neurons in **L**I and **L**II compared to all other layers. The sag ratio was computed by dividing the maximal voltage deflection by the mean steady state membrane potential, which was between -70 and -75 mV. **(D)** The rebound amplitude is significantly bigger in **L**I and **L**II principal neurons compared to that observed for principal neurons in the other layers. The amplitude is the difference between the maximum positive voltage deflection after offset of a negative current step and the resting membrane potential. **(E-F)** For the DAP, the difference between the amplitude of the depolarizing after potential and the amplitude of the threshold for firing was calculated. Note, that the DAP amplitude is bigger in **L**I and **L**II principal neurons compared to all other layers in response to a weak (E) and a +200 pA step (F). **(G)** No differences are observed in the rise time of the first AP in response to a weak current step, measured as the time to increase from 20 percent to the maximum AP amplitude to 80 percent. **(H)** The AP half-width measured at 50 percent of the AP amplitude of the first AP in response to a weak current step, is significantly smaller in **L**I and **L**II neurons compared to all other layers. **L**VI neurons have the significantly largest half-width.

Negative 200 pA injection triggers a prominent rebound potential at the end of the hyperpolarization step, inducing AP firing due to plateau depolarization in 25 percent of the neurons. Thirty-eight percent of the principal neurons are spontaneously active without current injection. MEC **L**I principal neurons can also have resonance properties (3.44 ± 1.02 Hz; Fig. $2C_3$; N=5) and membrane oscillations (3.06 ± 0.34 Hz; Fig. $2C_4$; N=4).

In general, basic physiological properties are comparable to those of MEC **L**II principal neurons (Figs. 3 and 4_1 versus $_2$). Next to principal neurons we recorded from neurons with the physiology of interneurons in **L**I (Suppl. Fig. 1A) with narrower APs and faster AP afterhyperpolarizations compared to principal neurons [35-37]. This paper does not provide further details on MEC interneurons.

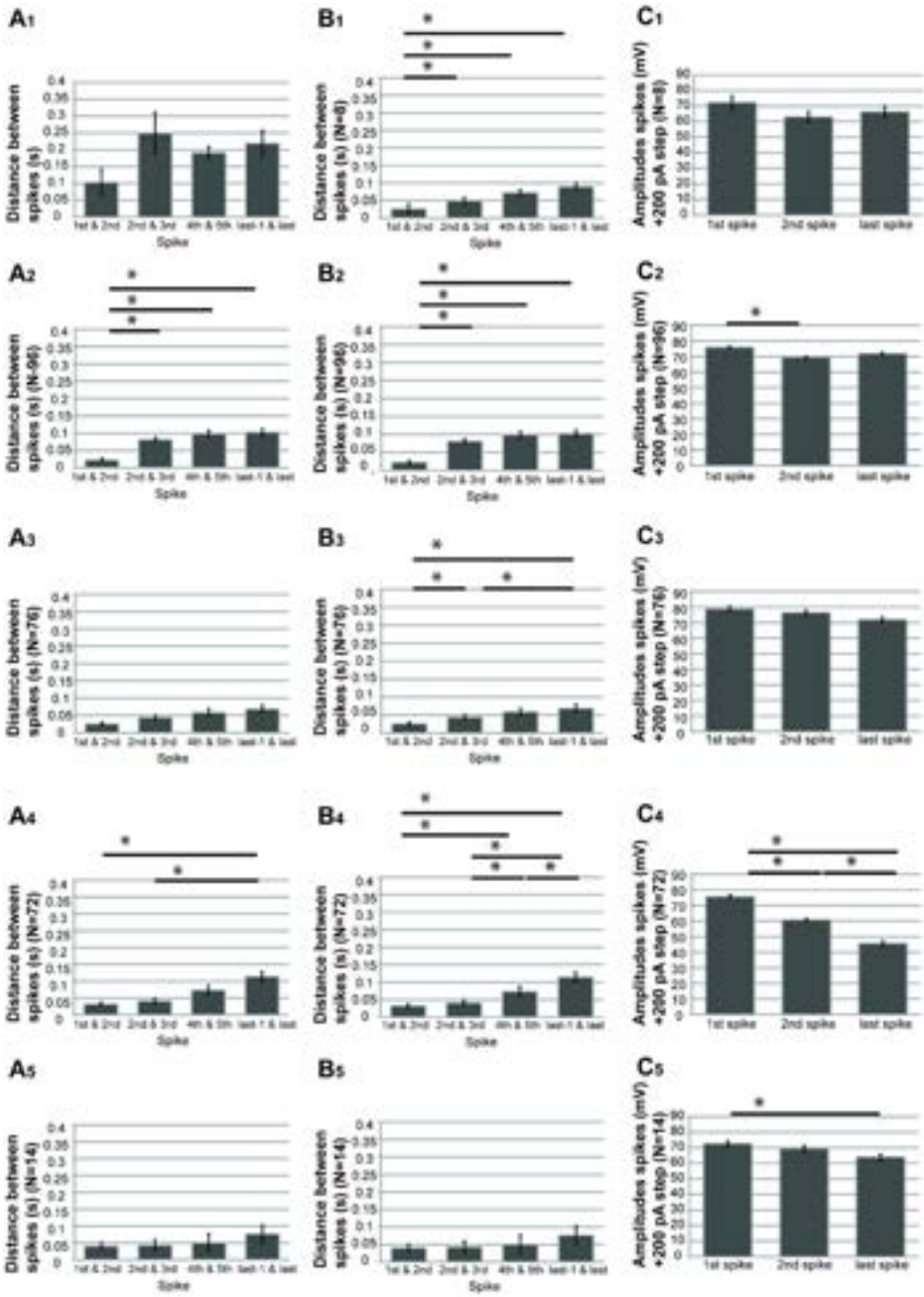

Figure 4: Histograms summarizing the ISIs of all layers in response to **(A)** a current step inducing at least six APs, and **(B)** to a +200 pA step. **(C)** AP amplitudes in response to +200 pA pulses. (A-C) Significance of $p < 0.05$ is indicated with *. On the y-axis, the parameter measured is indicated and the total number of neurons in which this parameter was measured (N=). Data are averages with the error bars indicating s.e.m.. (1-5) Represent the results for the principal neurons of the different layers, (1) **L**I, (2) **L**II, (3) **L**III, (4) **L**V, and (5) **L**VI. **(A-B)** The ISI is given for the 1st and 2nd

AP, the 2nd and 3rd AP, the 4th and 5th AP and the last and last-1 AP **(A)** Principal neurons in **L**I, **L**III and **L**VI do not show significantly different ISIs between APs in response to a weak current step, whereas **L**II and **L**V do. **(B)** Positive 200 pA injection leads to statistically significant differences in the ISI in all layers, except **L**VI. This indicates that principal neurons in all layers show SFA, except for **L**VI. SFA is the strongest in **L**V compared to the other layers. **(C)** The amplitude of the APs for the first, the 2nd and the last AP in a spike train in response to a +200 pA pulse. Amplitudes are measured as the difference between the AP threshold and the peak of the voltage deflection. The sizes of the APs do not decrease in **L**I and **L**III principal neurons. **L**II, **L**V and **L**VI principal neurons show a significant decrease in the amplitude from the 1st to the last AP, with **L**V neurons showing the strongest decrease in amplitude.

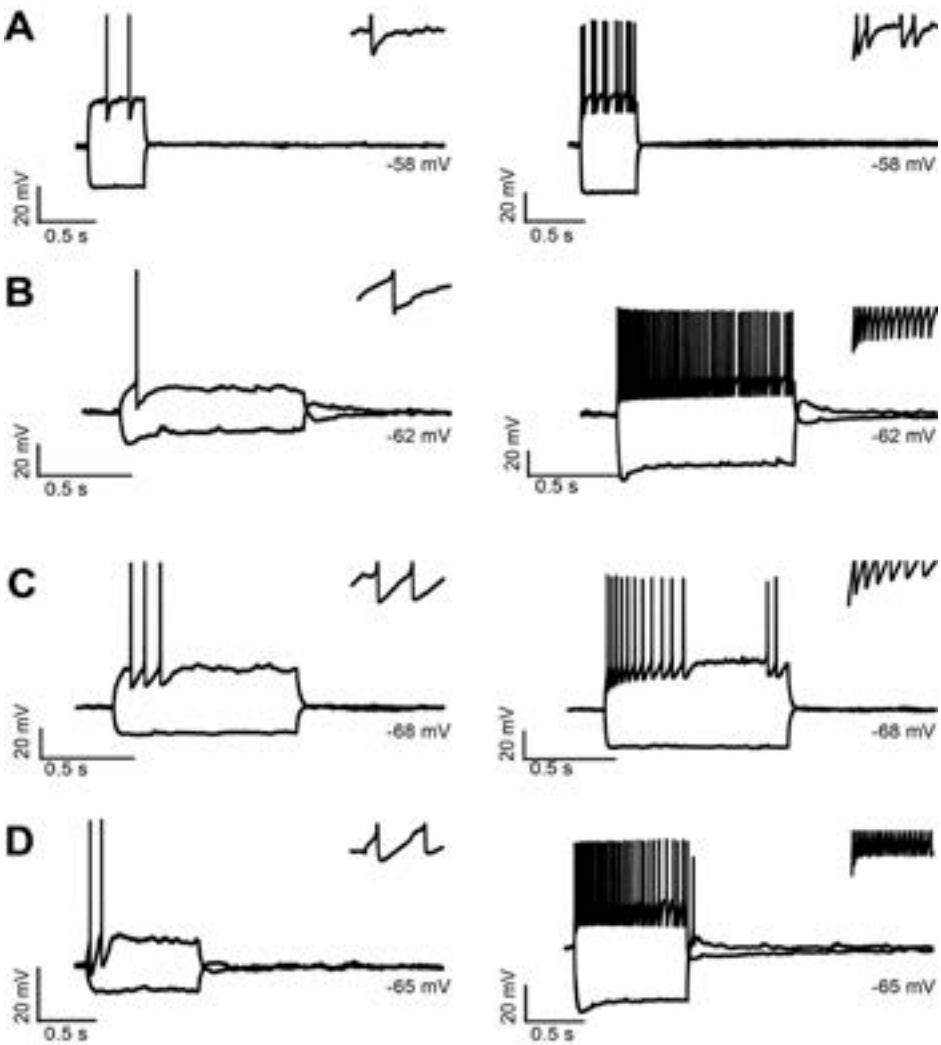

Supplementary Figure 1: Physiological profiles of MEC interneurons of different layers, **(A) L**I, **(B) L**II, **(C) L**III and **(D) L**V. (A-D) The voltage response of a representative interneuron to a weak hyperpolarizing and depolarizing step just reaching firing threshold is shown on the left side, and

to a ±200 pA step of 1 s on the right. In all subfigures the average membrane potential is indicated right below the individual voltage traces. Insets show a zoom in of 20 ms, displaying faster AP afterhyperpolarizations compared to principal neurons.

Layer II

Morphological properties.

LII of MEC contains two major and three intermediate morphological principal cell types. The main cell types are the stellate cells (SCs) and pyramidal neurons. The morphological and physiological properties of the two types have been described already in detail [16], and our findings corroborate the main findings of this report. We extend these findings, adding observations about the other intermediate cell types present. More importantly, we add a systematic analysis of the physiological properties of principal neurons at different mediolateral positions in MEC.

SCs in MEC are located throughout **L**II (Figs. 5A and 5B; N=53). They have two to 11 spiny primary dendrites leaving the somewhat rectangular or elongated soma primarily from the apex and from the side, and extending horizontally but also towards the pia, reaching a diameter of around 600 µm. The spiny basal dendrites travel within **L**II horizontally and towards deep layers, with a diameter of around 200 µm. They are shorter compared to the more apically directed dendrites but dendrites of 51 percent of the neurons reach **L**III. The main axon of SCs leaves directly from the soma and travels towards the angular bundle. A majority of collaterals are formed within the first 200 µm of the axon within deep **L**II and **L**III, without showing any preferred orientation or direction. The collaterals often split bidirectionally from the main axon with regular distance and angles, forming a net in **L**I-**L**III, covering an area of up to 900 µm in diameter when reaching the pia. Once at the pia the collaterals travel parallel to it. Sparse collaterals are also present in deep **L**III, the lamina dissecans and deep layers.

Pyramidal neurons (Figs. 5A and 5B; N=22) in **L**II have a pyramidal shaped soma with one sparsely spiny apical dendrite leaving the apex of the soma, bifurcating in **L**II and **L**I, reaching the pia, and covering around 300 µm in the horizontal direction. The sparsely spiny to spiny basal dendrites of pyramidal neurons spread in various directions for around 200 µm within **L**II and in 45 percent of the neurons they end in **L**III. The main axons of pyramidal neurons leave from the soma and travel to the angular bundle. Axon collaterals are formed mainly within **L**II and **L**III but they distribute mainly within **L**II and **L**I, reaching a diameter of up to 900 µm at the level of the pia.

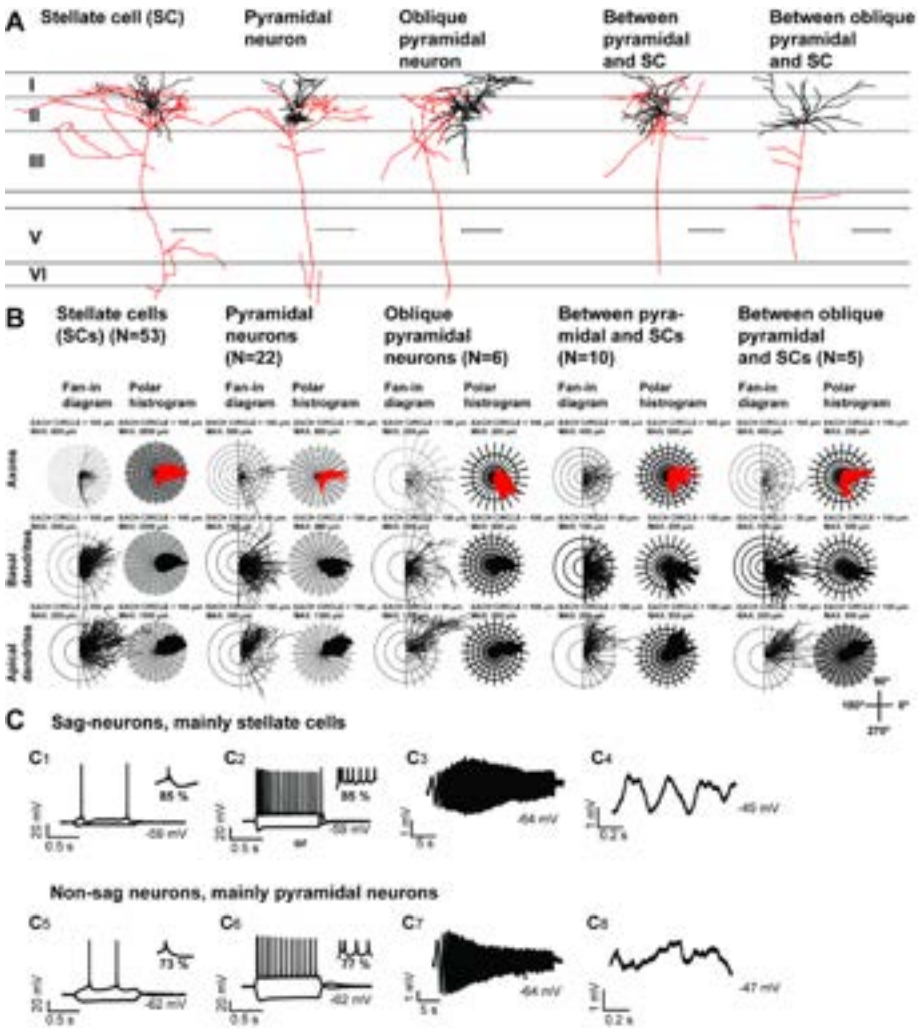

Figure 5: Morphology and physiology of MEC **L**II principal neurons. **(A)** From left to right, camera lucida drawings of a representative SC, pyramidal neuron, oblique pyramidal neuron, between pyramidal and SC, and a between oblique pyramidal and SC **L**II neuron. Horizontal lines indicate borders between layers of MEC. Dendrites are drawn black and axons red. Scale bars: 200 µm. **(B)** Morphological properties. Fan-in diagrams (left) and corresponding polar histogram plots (right) for each morphological subtype of the axons (top), basal dendrites (middle), and apical dendrites (bottom). The number of neurons (N=) is indicated. Note, that the polar plot of axons of all neuron types go towards deep and superficial MEC layers. **(C)** Most principal neurons have prominent sag potentials, rebound amplitudes, resonance properties and membrane potential oscillations (C_1-C_4). Pyramidal neurons and other subtypes do not have these properties (C_5-C_8). $\mathbf{C}_{1,\ 5}$. Voltage responses of two typical MEC **L**II principal neurons in response to a weak hyperpolarizing and depolarizing 1 s current step just reaching firing threshold. $\mathbf{C}_{2,\ 6}$. The voltage response to a ±200 pA step of 1 s. $\mathbf{C}_{1,\ 2,\ 5,\ 6}$. Insets show a zoom in of 20 ms displaying the AP afterpotentials. Below insets of $\mathbf{C}_{1,\ 2,\ 5,\ 6}$ the percentages of neurons with a DAP, for both

physiological cell types, are indicated. **C**$_{3, 7}$. Examples of voltage responses to a ZAP stimulus of the neurons that are also shown in C_1, C_2 and C_5, C_6, respectively. **C**$_{4, 8}$. Membrane fluctuations recorded just below firing threshold. In all subfigures the average membrane potential is indicated right below the individual voltage traces.

The first intermediate cell type is called oblique pyramidal neuron, which essentially looks like a tilted pyramidal neuron (Figs. 5A and 5B; N=6). They have pyramidal shaped somata with a horizontal orientation. Further they have one main spiny apical dendrite. The direction of the main apical dendrite towards the pial surface is determined by the tilt of the individual soma. The apical dendritic tree can extend up to 800 µm in the horizontal direction, which also holds for the axon. The spiny to sparsely spiny basal dendrites are thin, short, and spread in multiple directions from the soma, and they have extensive branches within deep **L**II and the most superficial portion of **L**III, reaching a diameter of 300 µm (Figs. 5A and 5B). The axon leaves the soma and travels towards the angular bundle. Collaterals leave the axon in the proximity of the soma and reach **L**III, **L**II and **L**I.

Two other intermediate cell types exist within **L**II. Both have a pyramidal shaped soma, but one has the apex facing the pia and the other one has a horizontally oriented soma. Both have multiple oblique and vertically oriented spiny apical dendrites, instead of just one main apical dendrite as described for pyramidal and oblique pyramidal neurons (Figs. 5A and 5B). Therefore these neurons have a morphology in between that of pyramidal, oblique pyramidal and SCs. The spiny to sparsely spiny apical dendrites of both intermediate types travel towards the pial surface and the spiny basal dendrites spread in multiple directions, reaching **L**III in 87 percent of the neurons. The maximum diameter of the apical dendritic tree at the level of and parallel to the pia is around 600 µm and that of basal dendrites around 300 µm. The axonal tree distribution does not differ from that of other **L**II principal neurons. Finally, the dendritic and axonal arbors of all **L**II principal neurons patched within 150 µm from the border with the parasubiculum do not cross this border (N=8). The dendrites of principal neurons patched at the border to LEC cross the border, extending into LEC for a short distance.

Electrophysiological properties.

LII principal neurons have a significantly lower input resistance and shorter time constant (tau) compared to principal neurons in **L**III-**L**VI, and the latter feature is also significantly shorter compared to **L**I principal neurons (Figs. 3A and 3B). The rise time of APs does not differ between layers (Fig. 3G), whereas the AP half-width is significantly smaller in **L**II (Fig. 3H) compared to **L**III-**L**VI principal neurons. The mean inter-spike-interval (ISI) for the first two spikes in response to weak and +200 pA injection is short (Figs. 4A_2 and 4B_2).

This is caused by the fact that the majority of principal neurons burst in the beginning of a spike train. Additionally, the second AP in a burst shows a significantly smaller amplitude compared to the first (Fig. $4C_2$). We further observed that principal neurons located superficially in **L**III, within 30 µm from the border to **L**II still have **L**II physiological and morphological properties (N=5). We have included those in our dataset of **L**II since morphologically they also resembled **L**II neurons.

Compared to LEC, MEC **L**II principal neurons have a significantly lower sag ratio ($p < 0.001$), shorter time constant ($p < 0.05$), bigger rebound amplitude ($p < 0.05$), quicker membrane oscillations ($p < 0.001$), higher resonance frequencies ($p < 0.001$) and a shorter ISI of the first and second spike in response to +200 pA injection ($p < 0.001$).

The majority of **L**II principal neurons are SCs. Eighty percent of SCs have a prominent sag potential with a sag ratio < 0.7 in the hyperpolarizing direction (Figs. 3C and $5C_2$) and 98 percent < 0.8. These neurons also have a rebound amplitude in the depolarizing direction (5.06 ± 0.44 mV; Figs. 3D and $5C_2$) with occasional APs on the top after offset of the hyperpolarizing current. In response to weak positive current steps, **L**II SCs have a sag potential in the depolarizing direction, and fire early in response to depolarization (Fig. $5C_1$). Eighty-five percent of SCs have a prominent measurable DAP in response to weak (3.29 ± 0.30 mV; Figs. 3E and $5C_1$) and +200 pA injection (4.25 ± 0.28 mV; Figs. 3F and $5C_2$). The remaining SCs have a DAP but it is small in amplitude and not measurable. SCs show bursting activity in response to weak and strong current injection followed by spike-frequency adaptation (SFA) and regular firing (Fig. $5C_2$). When neurons fire in a burst mode, the second AP is smaller in amplitude and does not have a DAP anymore but in 30 percent of the cases the third or fourth AP has one. In response to weak current injection the amplitude of DAPs decreases steadily from the first to the last AP, whereas in response to strong depolarization this can vary. Depolarization above -60 mV induces persistent and rhythmic membrane potential oscillations (3.81 ± 0.16 Hz; Fig. $5C_4$; N=46 out of 46) consistent with the apparent resonance (5.03 ± 0.16 Hz; Fig. $5C_3$; N=46 out of 46). A minority of eight percent of **L**II SCs shows spontaneous activity and ten percent show up and down states.

Pyramidal neurons in contrast do not show membrane potential oscillations (Fig. $5C_8$) and they do not have such strong resonance potentials as seen in SCs (3.62 ± 0.32 Hz; Fig. $5C_7$; N=14 out of 17). Seventy-three percent of pyramidal neurons have a small DAP in response to weak positive current injection (2.04 ± 0.52 mV) and 77 percent have DAPs in response to +200 pA injection (3.62 ± 0.55 mV), 41 percent have a sag ratio < 0.7, 86 percent < 0.8, and 36 percent have a small rebound (1.75 ± 0.13 mV). Neurons without a sag potential in the hyperpolarizing direction also do not have a sag potential in the depolarizing direction and thus they fire with a delay in response to weak

depolarization (Fig. $5C_5$). Neurons without a prominent DAP do not burst at the beginning of an AP train. In line with this, most pyramidal neurons fire regularly in response to weak depolarization and have a tendency to burst in response to strong depolarization.

The three intermediate principal neuron types have either the physiology of SCs or that of pyramidal neurons; 50 percent of the oblique pyramidal neurons and 73 percent of the other two intermediate cell types have membrane oscillations.

In vivo recordings of neuronal activity in freely moving rats showed that the majority of principal neurons in **L**II of MEC exhibit grid firing properties [8]. Recent *in vivo* studies have further indicated that grid scales increase progressively along the dorsoventral axis of MEC [38]. The existence of grid cell properties as well as the changes in firing scales, have been attributed to typical SC properties such as membrane oscillations and changes in their frequency respectively. Our observations did not clearly support a systematic change in membrane oscillatory characteristics related to dorsoventral levels and we therefore questioned whether this effect reported previously [15] might be masked due to variations along the mediolateral axis. We found that even within one slice, when patching up to four neurons simultaneously along the whole mediolateral axis, the differences between frequencies of membrane oscillations can be up to 3.2 Hz. We therefore systematically analyzed properties that are typical for **L**II principal neurons in MEC versus the location along the mediolateral axis of MEC neurons or extending this mediolateral axis across the border from MEC into LEC (Fig. 6). Analyzed properties include membrane oscillations, resonance frequencies, sag ratio, rebound amplitude, time constant, input resistance and DAP amplitudes.

All these properties show a trend to change in relation to the position along the mediolateral extent of MEC. When neurons in the adjacent part of LEC are included, these correlations are significant. Principal neurons at the MEC/LEC border and in LEC show membrane oscillations of a high frequency, which do not differ significantly from the oscillations in principal neurons positioned more medially in MEC ($df = 16$, $p = 0.564$). However, since the number of neurons without oscillations increases, the mean oscillation frequency shows a significant decrease along the mediolateral axis (Linear fit $R = 0.399$, $R^2 = 0.159$, $p = 0.000$, $F = 25.19$; slope -0.014; Fig. 6A; cf. [1]). Resonance frequencies of **L**II principal neurons change along the mediolateral axis ($R = 0.656$, $R^2 = 0.431$, $p = 0.000$, $F = 78.71$, slope = -0.025; 6B). The sag ratio increases from medial MEC to LEC ($R = 0.519$, $R^2 = 0.269$, $p = 0.000$, $F = 44.83$, slope = 0.001; Fig. 6C) with MEC principal neurons having a bigger sag amplitude compared to LEC neurons. The rebound amplitude decreases from MEC to LEC with principal neurons in medial MEC having a bigger rebound

amplitude compared to principal neurons in LEC (R = 0.234, R^2 = 0.055, p=0.008, F=7.295, slope = -0.234; Fig. 6D).

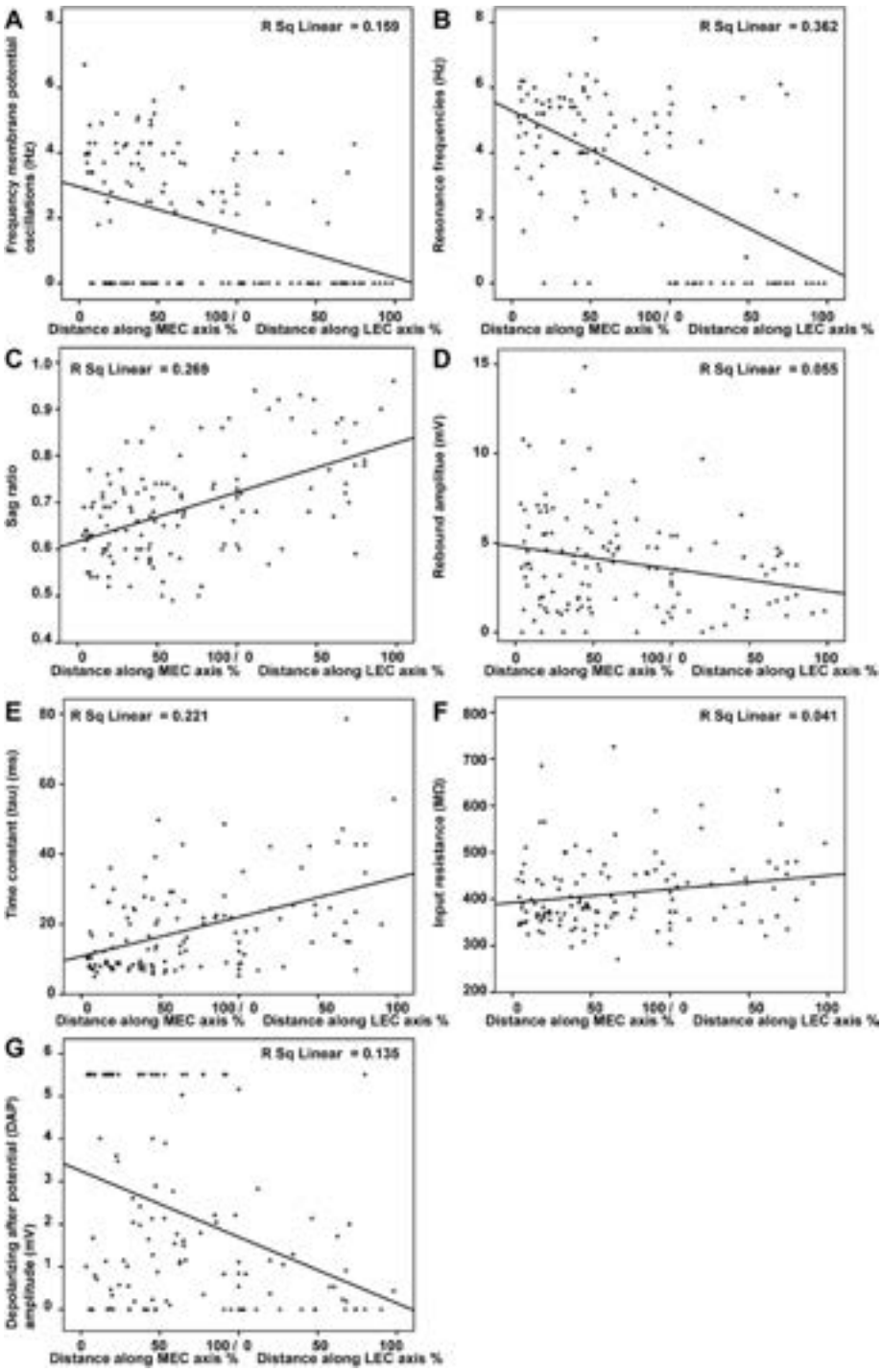

Figure 6: Differences in physiological properties along the mediolateral axis in MEC **L**II principal neurons. **(A)** The frequency of membrane potential oscillations, **(B)** the resonance frequency **(C)** the sag ratio **(D)** the rebound amplitude, **(E)** the time constant, **(F)** the input resistance **(G)** and the DAP amplitude after the first AP plotted versus the location along the mediolateral axis.

The time constant increases slowly but significantly from medial to lateral MEC (time constant: R = 0.30, R^2 = 0.09, p = 0.003, F = 9.101, slope = 0.30), and MEC to LEC (time constant: R = 0.470, R^2 = 0.221, p = 0.000, F = 36.29, slope = 0.112; Fig. 6E). The input resistance increases from MEC to LEC but only weakly (R = 0.202, R^2 = 0.041, p = 0.021, F = 5.42, slope=0.029; Fig. 6F). The DAP amplitude is largest in medial MEC compared to LEC (R = 0.367, R^2 = 0.135, p = 0.000, F = 19.47, slope = -0.015; Fig. 6G).

Layer III

Morphological properties.

This MEC layer harbors a total of five different principal neurons. Small spiny pyramidal neurons are located throughout **L**III (Figs. 7A and 7B; N=14). The somata are pyramidally shaped with one spiny apical dendrite that leaves at the apex of the neuron, extending to the pia. On its way it divides occasionally in superficial **L**III and more often in **L**II such that the apical tuft in **L**I covers an area of up to 600 µm in diameter parallel to the pia. In the majority of these neurons the spiny basal dendritic tree with a final diameter of up to 500 µm distributes in multiple directions. In a minority (N=2) the basal dendrites reach only towards deep layers. The axons of the small neurons travel straight towards the angular bundle forming collaterals from deep **L**III onwards reaching both **L**II and deep layers.

Complex pyramidal neurons are mainly located in deep and middle **L**III (Figs. 7A and 7B; N=35). Seventy-one percent of the neurons have a pyramidally shaped soma. The others have round to elongated somata. Complex pyramidal neurons, in contrast to small spiny pyramidal neurons, can have two primary spiny apical dendrites that leave the apex. The apical dendrite branches frequently within **L**III. The apical dendritic arbor can reach its maximum diameter of up to 400 µm already in **L**III, in contrast to the small spiny pyramidal apical dendritic tree that maximizes its diameter in **L**I. The spiny basal dendritic tree has a diameter of about 400 µm. The basal dendrites of complex pyramidal neurons are generally confined to **L**III, rarely reaching **L**V (N=3). The main axon of complex pyramidal neurons travels towards the angular bundle and sometimes into the subiculum. Many collaterals are formed and spread within **L**III and the lamina dissecans. Other collaterals travel via deep MEC layers towards very superficial **L**I. The diameter of the axonal tree, as measured in a plane parallel to the pia, can reach a diameter of up to 800 µm.

The round somata of multipolar principal neurons are located in middle to deep **L**III (Figs. 7A and 7B; N=6), mainly very medially close to the border with the parasubiculum (Fig. 1). The sparsely spiny to spiny multipolar dendritic tree of those neurons distributes within deep **L**II, throughout **L**III, and the lamina dissecans and can have a diameter of up to 400 µm. The axons of multipolar neurons leave the soma and branch within **L**III and **L**V. Collaterals can distribute into superficial **L**I (N=1) but are mainly confined to a volume with a diameter of 400 µm in **L**III-**L**V. The main axon travels towards the angular bundle. Multipolar, but also pyramidal neurons located at the border to the parasubiculum can have parts of their basal dendrites and axons traveling into the parasubiculum (N=4).

A fourth cell type located in superficial **L**III is the SC (N=10). They have one frequently splitting sparsely spiny to spiny apical dendrite leaving a pyramidal shaped soma (Figs. 7A and 7B). At the pia, the dendrites reach a diameter of up to 600 µm. The sparsely spiny to spiny basal dendritic tree is multipolar and remains within superficial **L**III and reaches a horizontal diameter of around 250 µm. The axon travels towards the angular bundle having only few collaterals compared to other **L**III principal neurons.

The last morphological type, the bipolar complex pyramidal neuron, has up to two apical dendrites that leave the round to pyramidally shaped soma at the apex extending towards the pia and one dominant basal dendrite that branches horizontally within **L**III, occasionally reaching superficial **L**V (Figs. 7A and 7B; N=4). The spiny basal dendritic arbor of the bipolar neurons can have a diameter up to 800 µm horizontally. The apical dendritic tree is smaller but still reaches a diameter of 600 µm horizontally. The bipolar complex pyramidal neurons are mainly located in middle or deep **L**III. The axon of bidirectional pyramidal neurons collateralizes frequently within **L**III or in the lamina dissecans, extending in these two layers before entering superficial and deep layers. The diameter of the axons can occasionally reach up to 700 µm in a plane parallel to the pia.

Electrophysiological properties.

Within **L**III the morphological neuron types do not differ significantly regarding their physiology. The input resistance of **L**III principal neurons is in between those of principal neurons in **L**V and **L**II (Fig. 3A). The time constant is slower than that of **L**II and **L**I principal neurons (Fig. 3B). None of the **L**III principal neurons have a sag ratio < 0.8 (Fig. 3C), or a prominent rebound amplitude (Figs. 3D, and $7C_{1, 2, 4, 5}$). Positive 200 pA injection leads to a DAP in five neurons (Figs. 3E and 3F). **L**III principal neurons have significantly wider APs compared to **L**II principal neurons but narrower compared to principal neurons in deeper layers (Fig. 3G).

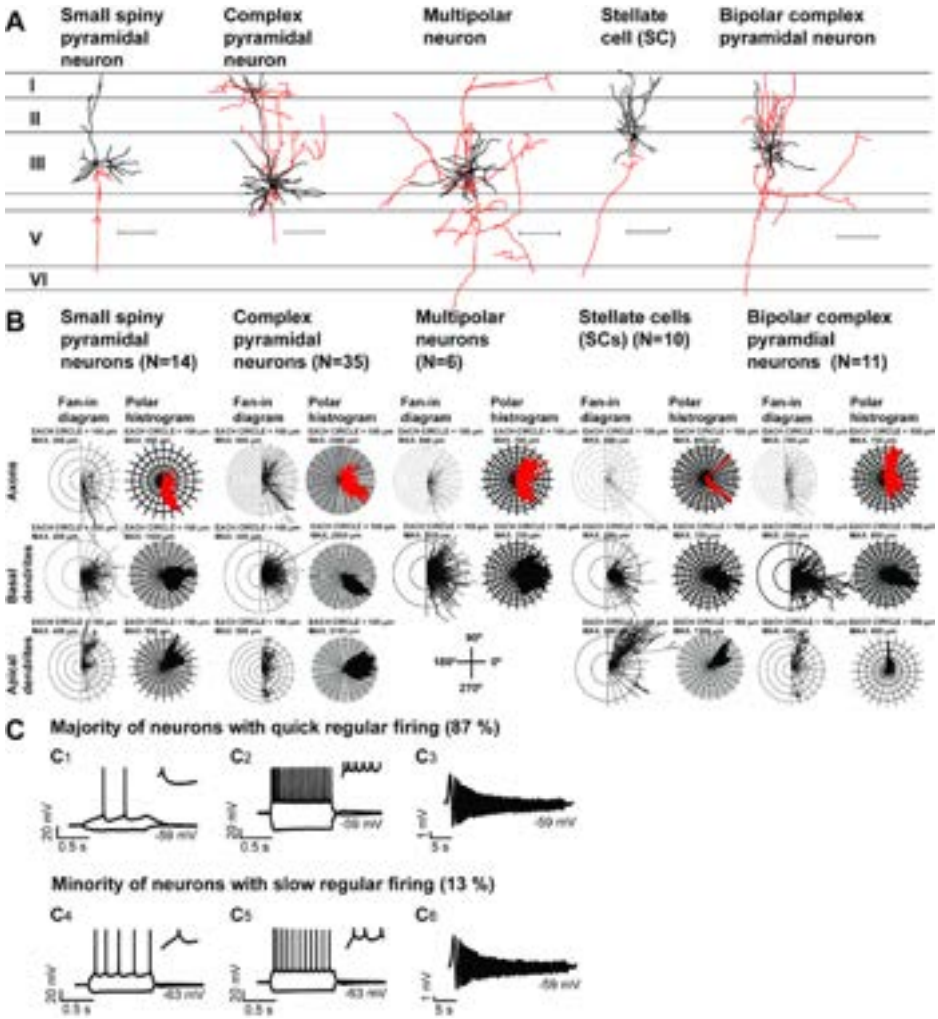

Figure 7: Morphology and physiology of MEC **L**III principal neurons. **(A)** From left to right, camera lucida drawings of a representative small spiny pyramidal neuron, a complex pyramidal neuron, a multipolar neuron, a SC, and a bipolar complex pyramidal neuron with one prominent horizontal dendrite. Horizontal lines indicate borders between layers of MEC. Dendrites are represented in black and axons in red. Scale bars: 200 µm. **(B)** Morphological properties. Fan-in diagrams (left) and corresponding polar histograms (right) for each morphological subtype of the axons (top), basal dendrites (middle) and apical dendrites (bottom). The number of neurons (N=) is indicated. Note, the apical dendrites of complex pyramidal neurons split more frequent after leaving the soma compared to the simple neurons (fan-in diagrams). The axonal arbors of **L**III neurons travel towards superficial and deep layer. **(C)** **L**III principal neurons do not have a prominent sag potential, rebound amplitude and resonance. In response to weak current injection principal neurons fire with a delay. Positive 200 pA injection leads to SFA (**C**$_2$) or not (**C**$_5$). **C**$_{1, 4}$. Voltage responses of two typical MEC **L**III principal neurons in response to a weak hyperpolarizing and depolarizing 1 s current step just reaching firing threshold. **C**$_{2, 5}$. The voltage response to a ±200

pA step of 1 s. **C**$_{1, 2, 4, 5}$. Insets show a zoom in of 20 ms, displaying the AP afterpotentials. **C**$_{3, 6}$. Examples of voltage responses to a ZAP stimulus of the neurons that are also shown in C_1, C_2 and C_3, C_4, respectively. In all subfigures the average membrane potential is indicated right below the individual voltage traces.

Principal neurons in **L**III of MEC do not differ significantly from those in LEC with respect to the input resistance, time constant, sag ratio, rebound and DAP amplitudes, as well as the AP rise time and half-width. In response to weak current injection, **L**III neurons fire with a delay, the evoked firing pattern is regular, with weak SFA (Figs. 4A_3 and 7C_4). Positive 200 pA injection leads to significant SFA (Figs. 4B_3 and 7$C_{2, 5}$). At the beginning of the depolarization step, 87 percent of **L**III principal neurons fire with a high frequency (Fig. 7C_2) but after the first couple of APs neurons fire more regularly (Fig. 4B_3). The amplitude of the APs does not change significantly from the first to the last AP (Fig. 4C_3). Sixty-five percent of the neurons show an activity hump meaning that the membrane and the amplitude of the APs increase within the first 50 ms followed by a decrease to a steady state level (Fig. 7C_2). Generally, **L**III principal neurons do not have membrane oscillations and they do not resonate (Figs. 7$C_{3, 6}$), but we found three principal neurons with oscillations between 7-8 Hz, which are not regular and consistent. Multipolar and complex pyramidal neurons can show spontaneous activity (N=8), occasionally leading to consistent up and down states (N=3).

Lamina dissecans

Neurons located in the lamina dissecans can either have the morphology and physiology of **L**III or **L**V principal neurons and were therefore included into the groups of these layers respectively.

Layer V

Morphological properties.

Putative principal neurons within **L**V of MEC can be morphologically divided into four different types. The first type, the superficially located pyramidal neurons, which have larger cell bodies compared to pyramidal neurons located in deep **L**V [39], can be subdivided into two subtypes either having a multidirectional (Fig. 8B; N=27) or horizontal sparsely spiny basal dendritic tree (Figs. 8A and 8B; N=6). Superficial pyramidal neurons have large pyramidal to round shaped cell bodies and one distinct spiny apical dendrite that reaches the pia. The apical dendrite branches occasionally close to the soma in the lamina dissecans and then again from **L**II up to **L**I.

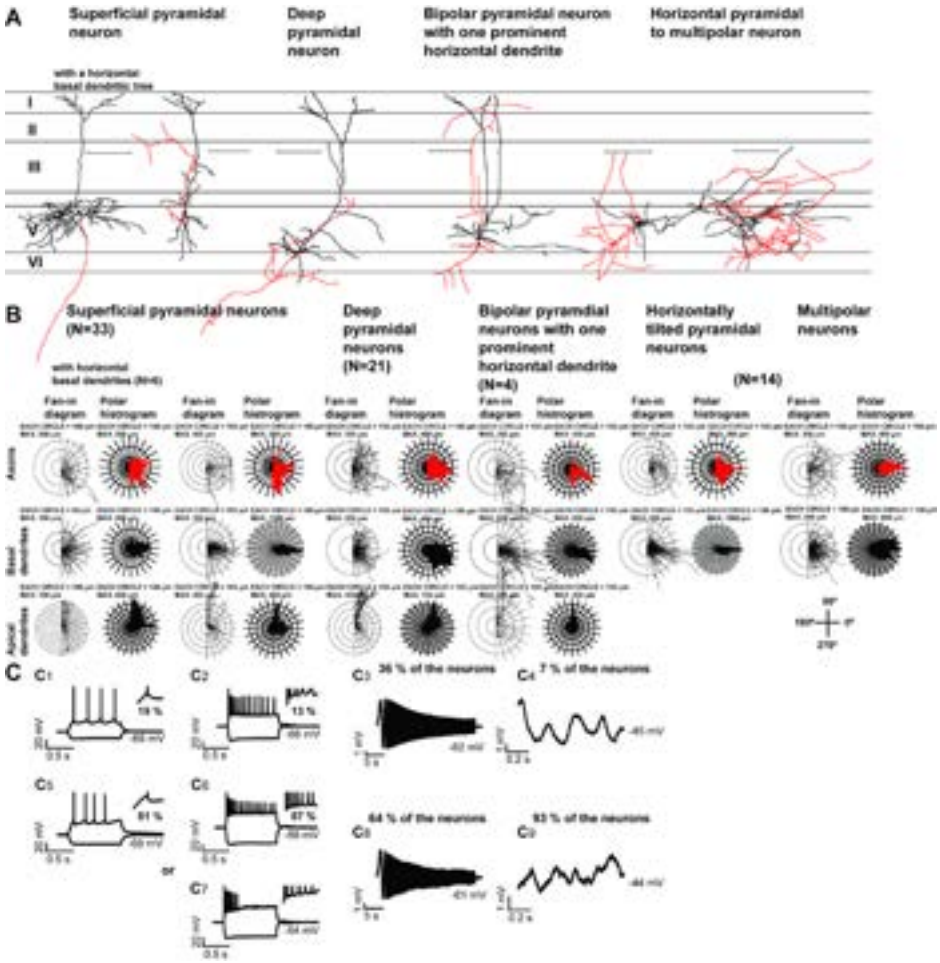

Figure 8: Morphology and physiology of MEC **L**V principal neurons. **(A)** From left to right, camera lucida drawings of two superficial pyramidal neurons with or without a prominent horizontal basal dendritic tree, a pyramidal neuron located in deep **L**V, a bipolar pyramidal neuron with one prominent apical and one prominent basal dendrite, and two multipolar **L**V principal neurons. Horizontal lines indicate borders between layers of MEC. Dendrites are represented in black and axons in red. Scale bars: 200 µm. **(B)** Morphological properties. Fan-in diagrams (left) and corresponding polar histogram plots (right) for each morphological subtype of the axons (top), basal dendrites (middle) and apical dendrites (bottom). The number of neurons (N=) is indicated. Note, that the axons can travel towards deep and superficial layers **(C)** Weak depolarization induces relatively regular firing in **L**V neurons. Positive 200 pA depolarization induces SFA, sometimes correlated with a constant decrease in the AP amplitude. The majority of neurons do not have membrane potential oscillations and a resonance. $\mathbf{C}_{1,\,5}$. Voltage responses of typical MEC **L**V principal neurons in response to a weak hyperpolarizing and depolarizing 1 s step just reaching firing threshold. $\mathbf{C}_{2,\,6,\,7}$. The voltage response to a ±200 pA step of 1 s. $\mathbf{C}_{1,\,2,\,5,\,6,\,7}$. Insets show a zoom in of 20 ms, displaying the AP afterpotentials. Below inset in $\mathbf{C}_{1,\,2}$ the percentage of

neurons with or **C**$_{5, 6}$ without a DAP are indicated. **C**$_3$. Examples of voltage responses to a ZAP stimulus of the neurons that are also shown in C_1, C_2 and C_5, C_6, respectively. **C**$_{4, 9}$. Membrane fluctuations measured below firing threshold. Above each of the traces **C**$_{3, 4, 8, 9}$ the number of neurons with this characteristic is written. In all subfigures the average membrane potential is indicated right below the individual voltage traces.

Within **L**I the diameter of the apical dendritic tree can be up to 400 µm. Less dendrites branch off in **L**II-**L**III compared to **L**I and make the tree-diameter in these layers much smaller. The spiny to sparsely spiny basal dendrites extend either profusely in all directions within **L**V and **L**VI (N=3) or only within **L**V (N=24). The basal dendritic tree diameter is often wider compared to the apical one and can reach a diameter of up to 700 µm in the laminar plane. The main axon is directed towards the angular bundle. Collaterals distribute within **L**V and occasionally extend into superficial **L**II. The axons reach superficial layers in the proximity of the apical dendrite having a maximum distance from the apical dendrite of up to 200 µm.

Deep pyramidal neurons are located throughout most of **L**V with the exception of the very superficial portion. They have smaller somata compared to superficial pyramidal neurons and a sparsely spiny apical dendrite that reaches the pia, forming dendritic branches in superficial **L**III in eight percent of the neurons (Figs. 8A and 8B; N=21). In the majority of neurons, the apical dendrite branches in **L**II and **L**I, reaching a diameter of 200-300 µm. Multiple sparsely spiny basal dendrites leave the soma towards all directions (N=13) or horizontally (Fig. 8B; N=8), and generally extend within **L**V and superficial **L**VI (N=4) with a horizontal diameter of up to 300 µm. The axons of these neurons extend into the angular bundle forming collaterals within **L**V and **L**VI. Additional collaterals travel up to **L**II in the proximity of the apical dendrite.

Bipolar pyramidal neurons with one apical and one prominent basal dendrite that travels within **L**V parallel to the border with the lamina dissecans, form the third type. The sparsely spiny apical dendrite generally has some small branches already close to the soma and on the way to **L**I, multiple small branches are coming off. In LI a clear apical tuft is present (Figs. 8A and 8B; N=4). The sparsely spiny to spiny basal dendritic tree extends unidirectional from the soma with a diameter of 700 µm. The axon reaches the angular bundle and collaterals are formed in deep layers and can travel up to **L**I.

The last morphological neuron group comprises multipolar (N=5) and tilted pyramidal neurons (N=9). Those neurons have in common that the sparsely spiny to spiny dendritic tree splits mainly within deep layers and does not reach superficial layers (Figs. 8A and 8B). Multipolar neurons have dendrites facing all directions with a similar length. Tilted pyramidal neurons have one main dendrite that extends either horizontally to the border with or into **L**VI. This dendrite can travel up to 700 µm horizontally within **L**V. The axons of both

neuronal types form collaterals mainly in deep layers. The collateral can occasionally reach **L**II in the vicinity of the soma, rarely extending further out up to 700 µm.
Any of the **L**V principal neuron types, if located close to the border with the parasubiculum, occasionally has dendrites (N=4) and axons (N=1) that cross this border.

Electrophysiological properties.
Independent of morphological properties, **L**V principal neurons have a higher input resistance compared to all other layers (Fig. 3A) and a shorter time constant compared to **L**II (Fig. 3B). The AP rise time does not differ compared to that of principal neurons of other layers (Fig. 3G), whereas the AP half-width is significantly larger compared to **L**I-**L**III principal neurons (Fig. 3H). They do not show prominent differences compared to LEC **L**V principal neurons, except that in MEC the AP half-width is larger and the rise time is slower than in LEC. Eight percent of **L**V principal neurons have a prominent sag ratio < 0.7 and 24 percent have a sag ratio < 0.8 (Figs. 3C and $8C_2$). The neurons with lower sag ratios have larger rebound amplitudes (Figs. 3D and $8C_2$). In response to weak and +200 pA injection **L**V neurons show SFA (Figs. $4A_4$ and $4B_4$). Nineteen percent of the principal neurons have a DAP in response to weak current injection, but only after the first AP (Figs. 3E and $8C_1$ inset). Having a DAP does not however implicate the existence of a sag potential. In 13 percent of the neurons +200 pA injection induces a DAP after the first AP (Figs. 3F and $8C_2$ inset). This further results in immediate firing and a decrease in the AP amplitude especially from the 1st to the last AP (Figs. $4C_4$ and $8C_{2,\ 6,\ 7}$). Thirty-six percent of **L**V principal neurons have resonance properties of 1.3 ± 0.4 mV (Fig. $8C_3$) and of those neurons, seven percent show membrane oscillations between 4 and 7.3 Hz (Fig. $8C_4$). Seventeen percent of **L**V principal neurons have the tendency to be spontaneously active. We recorded from three principal neurons that were located very superficially in **L**VI and they show the physiological and morphological profile of **L**V neurons. Therefore we classified them here as **L**V principal neurons although they could also be classified as a subtype of superficial **L**VI principal neurons.

Layer VI
Morphological properties.
In **L**VI two morphologically different putative principal neurons were observed, pyramidal and multipolar neurons. Pyramidal neurons have a pyramidal to round shaped soma with either a prominent sparsely spiny to spiny dendrite traveling parallel to the layers with no prominent apical dendrite reaching superficial MEC layers (Fig. 9A; N=7), or they are completely tilted and the dendrites face towards the subiculum (Fig. 9A; N=4).

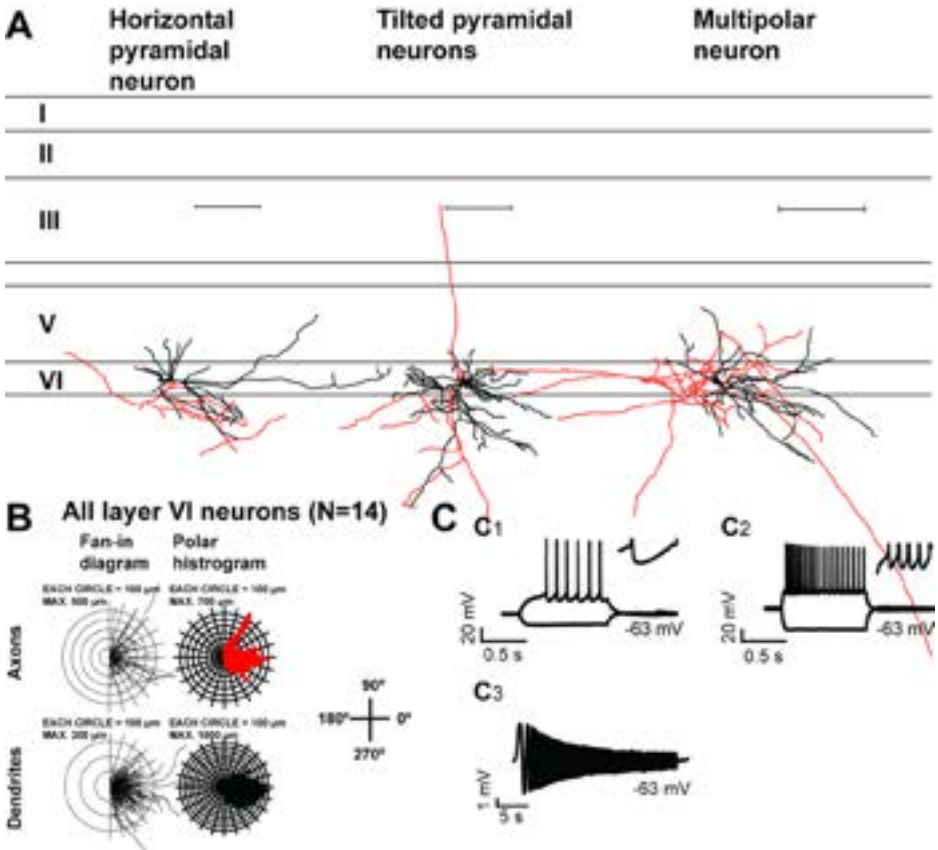

Figure 9: Morphology and physiology of MEC **L**VI principal neurons. (A) From left to right, camera lucida drawings of a horizontal pyramidal neuron, a tilted pyramidal neuron and a multipolar **L**VI principal neuron. Lines indicate borders between layers of the MEC. Dendrites are represented in black and axons in red. Scale bars: 200 µm. (B) Morphological properties. Fan-in diagrams (left) and corresponding polar histogram plots (right) for all **L**VI neurons patched of the axons (top) and dendrites (bottom). The number of neurons (N=) is indicated. Note, that **L**VI principal neurons project to superficial layers (axons) but that the dendritic tree remains within deep layers. (C) **L**VI principal neurons fire very regular without a sag potential, rebound amplitude, DAPs or resonance properties. C_1. The voltage response of a typical **L**VI principal neuron to a weak hyperpolarizing and depolarizing 1 s current step just reaching firing threshold. C_2. The voltage response to a ±200 pA step of 1 s. C_1 and C_2. Insets show a 20 ms zoom in, displaying the AP afterpotentials. C_3. Example of a voltage response to a ZAP stimulus of the neuron that is also shown in C_1 and C_2. In all subfigures the average membrane potential is indicated right below the individual voltage traces.

Multipolar principal neurons have sparsely spiny to spiny dendrites of similar length extending in all directions (Fig. 9A; N=3). With the exception of the latter the dendrites of **L**VI neurons stay within deep layers and rarely reach deep

LIII. The dendritic tree can be up to 800 µm in diameter as measured parallel to the layer. Axons collateralize within **L**V-**L**VI, the angular bundle, and the subiculum and can travel towards superficial layers, reaching deep **L**II.

Electrophysiological properties.
Principal neurons in **L**VI have a different physiology from **L**V principal neurons in that they have input resistances (Fig. 3A) and time constants (Fig. 3B) comparable to **L**III principal neurons. Additionally **L**VI principal neurons do not have sag potentials (Fig. 3C), no rebound amplitudes (Fig. 3D) in response to hyperpolarization, no DAPs after APs (Figs. 3E, 3F, and $9C_{1, 2}$ insets), no membrane potential oscillations and no resonance (Fig. $9C_3$). They fire with a delay in response to weak current injection (Fig. $9C_1$). **L**VI principal neurons fire very regularly with a frequency of around 10-20 Hz (Figs. $4A_5$ and $4B_5$). In an AP train the amplitudes of APs show a slight constant decrease (Fig. $9C_2$), which leads to a significant decrease in the AP amplitude from the 1st to the last AP (Figs. 9C and $4C_5$). Compared to **L**I-**L**III, **L**VI principal neurons have significantly wider APs (Fig. 3H). MEC and LEC **L**VI principal neurons differ in that the input resistance and time constant of MEC **L**VI principal neurons is significantly higher ($p < 0.013$) and slower ($p < 0.05$), respectively.

3.3 DISCUSSION

For this study we performed *in vitro* whole cell current-clamp recordings from multiple individual neurons allocated to one of the MEC layers and compared the morphological and physiological characteristics within and between cell layers. This is the first study reporting on morphological and physiological properties of MEC **L**I-**L**VI principal neurons under standardized conditions and throughout most of the dorsoventral and mediolateral MEC axes for all layers.
We draw four main conclusions from this study. First, within different MEC layers a unique set of morphologically defined principal neurons exists. Second, with the exception of **L**II neurons, within all MEC layers the different morphologies of principal neuron types do not implicate a specific associated physiology. Third, physiological characteristics of principal neurons are layer specific. Fourth, our data show that **L**II principal neurons display a mediolateral gradient with respect to some of the **L**II specific physiological properties. We show that this gradual change in physiological properties continuous into adjacent LEC. Finally, a comparison between the data obtained in both MEC and LEC (see also the accompanying paper [1]), suggests that the main neuronal differences between both entorhinal subdivisions are to be found in **L**II.

1. Layer and cell type specific morphology: relevance for integrative properties

Layer I. MEC **L**I contains mainly fibers and interneurons [40, 41] but we also recorded from neurons with axons extending into the angular bundle. These **L**I neurons are thus likely principal neurons. **L**I neurons have been described to project to the hippocampus, but these were immunoreactive for GABA and thus inhibitory [42]. In contrast, the physiological properties of the neurons we recorded from indicate them to be excitatory [35]. This suggests that **L**I comprises both inhibitory and excitatory projection neurons, in line with previous anatomical observations that some **L**I neurons are not immunoreactive for GAD or GABA [43]. It remains to be established, whether GABAergic neurons project exclusively to the hippocampal formation and the excitatory projection neurons project outside the hippocampus.

Morphologically, **L**I neurons receive most of their input from presynaptic endings in **L**I, since most of their dendritic trees are confined to **L**I. Their axon, on the way to the angular bundle, does not collateralize extensively, indicating that **L**I neurons do not communicate a lot with peer **L**I neurons or with neurons in any other layer. All these morphological properties are similar to what we have shown for LEC **L**I [1], except that the amount of spines found on MEC **L**I neurons is lower. Although **L**I principal cells in MEC share several morphological properties with those in **L**II, the differences in axonal distribution and spine density suggest that **L**I principal neurons form a cell type separate from **L**II neurons.

Layer II. In line with previous reports, we divided MEC **L**II principal neurons into two main cell types, namely SCs and pyramidal neurons, and three intermediate cell types [16, 21, 44, 45]. Our data on the morphologies of these cell types generally corroborate those previously published. Regarding the three intermediate principal neuron types, Gatome (2010) showed that these different cell types do not have a preferred distribution along the mediolateral axis of MEC, which is corroborated by our observations. The common denominator of all studies is that in MEC the majority of **L**II neurons have a SC morphology. In contrast, in LEC morphologically different neurons are represented in equal percentages [1, 46].

In a recent *in vivo* study [47], data on one completely reconstructed SC were reported. The majority of axonal collaterals were found throughout **L**I (90.7 percent) spanning 1280 µm in the mediolateral and 2266 µm in the dorsoventral extend. The remaining axonal collaterals were found in **L**II and **L**III. Our data indicate that pyramidal neurons in **L**II have a broadly extending axonal tree similar to that of SCs and this is in contrast to a previous report that pyramidal cells have a smaller axonal tree [16]. All available data thus

suggest that **L**II SCs as well as pyramidal cells make the majority of their contacts with postsynaptic sites in **L**I, followed by postsynaptic sites in **L**II. This strongly suggests that **L**II neurons communicate extensively with postsynaptic targets in **L**I and **L**II, be it principal neuron or interneuron [47-49]. Based on the overall extend of the axonal arbor, the capacity for local interactions of MEC **L**II neurons is more extensive than in case of LEC **L**II principal neurons [1, 46].

Layer III. Within **L**III we defined small spiny pyramidal neurons and complex pyramidal neurons thus corroborating previous reports. The main new observation is that the distribution of the axonal tree of the complex cells in our study is more extensive [18, 21, 50], likely reflecting differences in preservation of the axon in differentially cut slices. Having a more extensive axonal arbor is in line with recent *in vivo* data that indicate an even more extensive distribution (1668 µm in the dorsoventral axis and 520 µm in the mediolateral axis [47]). The *in vivo* data further indicate that up to 27 percent of the axonal tree extends into **L**V, which is not reported in any of the slice studies.

A minority of neurons are multipolar principal neurons, which are mainly located medially, close to the border with the parasubiculum. Dendrites and axons of multipolar and pyramidal neurons close to the border do cross the border, indicating that they may receive inputs targeting the parasubiculum.

The dendritic distribution of the majority of MEC **L**III principal neurons suggests that they potentially integrate inputs coming into **L**I, **L**II and **L**III. The basal dendrites of only a minority of the neurons reach **L**V (11 percent; see also [18, 21, 47, 50]). Thus a small selection of **L**III neurons can potentially receive retrosplenial, cingular, pre- and infralimbic inputs that are essentially confined to **L**V. This is a clear difference compared to LEC, where more **L**III principal neurons have basal dendrites in **L**V ([46]: 32 percent; [1]: 44 percent) but a less prominent horizontal dendritic tree within **L**III. Hippocampal input that distributes to both **L**V and **L**III will likely target **L**III neurons in both entorhinal subdivisions with an equal likelihood [51].

The extension of the axonal plexus indicates that MEC **L**III principal neurons predominantly interact with peer MEC **L**III neurons [48] likely including both principal neurons and interneurons [47]. Collaterals also reach **L**I and **L**V [50] but details on postsynaptic targets are not known. For a number of principal neurons we observed that the axonal arbor can be wider than that of the corresponding dendritic tree because at least one collateral travels horizontally from the soma and then collaterals extend superficially. This morphological feature predicts that **L**III principal neurons transfer information to **L**II with a certain directional preference, in line with recently reported *in vitro* observations [52] and corroborating postulated asymmetrical deep to superficial connectivity in attractor dynamic-based theoretical accounts on the emergence of grid cell firing in **L**II of MEC [11]. Neither the extended spread of the axonal

arbor nor the directionality has been observed in case of LEC **L**III principal neurons [1, 46].

Layer V. Pyramidal neurons form the majority of principal neurons in MEC **L**V, and these neurons have been described by several authors [22, 39, 47, 53]. A striking feature of these neurons is the pronounced apical dendrite extending to the pial surface. In contrast to reports by Lorente de Nó (1933) and Hamam *et al.* (2000) who found that the apical dendrites of **L**V neurons do not start branching before reaching **L**II, we observed that the apical dendrites of pyramidal neurons start branching in **L**III in 14 percent of the neurons. All accounts agree that the basal dendrites of pyramidal neurons generally show either a horizontal or multipolar organization. The extent of the basal dendritic tree is very wide in the laminar direction up to 800 µm within MEC **L**V. Thereby **L**V pyramidal neurons can receive inputs from many other **L**V neurons but also from axons that pass **L**V on their way to superficial or deep layers. It is apparent that more neurons with a horizontally located basal dendrite exist in MEC compared to LEC [1, 22, 54].

In line with single cell *in vivo* data [47], but in contrast to a previous *in vitro* study [22], we observed that for the majority of **L**V pyramidal neurons the axons travel towards superficial layers. Slice studies such as ours clearly underestimate the total distribution in case of extensive axonal trees since *in vivo* measures indicate an extent of 2748 µm in the dorsoventral axis and 2044 µm in the mediolateral axis [47].

Within **L**V there are also principal neuron types that have their dendrites only in deep layers and therefore they can potentially only receive inputs that enter the deep layers. Hamam *et al.* (2000) showed that **L**V principal neurons can also have their apical dendrites within subiculum but we have not been able to confirm that although we have seen a similar morphology in case of **L**VI principal neurons.

In accordance with a previous *in vivo* report [23], we observed a cell type in **L**V that has one apical dendrite up to the pia and a few basal dendrites directed towards the angular bundle. Since these basal dendrites may extend as far as the subiculum [23], the bipolar neurons may integrate incoming or local activity across all layers of MEC and subiculum [20, 39].

In conclusion, **L**V principal neurons can potentially receive inputs that distribute in any layer from **L**I down to **L**VI and this has recently been found to hold true regarding inputs from the pre- and parasubiculum that selectively distribute to **L**I/**L**III and **L**II, respectively [55, 56]. **L**V principal neurons can also transfer the information to all layers in MEC, but mainly within **L**V and **L**III [47]. In addition to the prevailing view on **L**V principal neurons as distributing hippocampal output, our data indicate that neurons in **L**V are the main integrators and local distributors in MEC. The morphology of most MEC and

LEC **L**V principal neurons is very similar, therefore it is likely that LEC **L**V neurons play a comparable integrative role.

Layer VI. Principal neurons in **L**VI seem to be functionally different from all other MEC neurons since their morphology suggests that their major input is from axons that terminate in **L**V, **L**VI, subiculum, or pass through the angular bundle [23]. They are thus the potential candidates to integrate the results of local entorhinal processing in the deep layers with ongoing activity in the subiculum. The unique characteristic is further strengthened by the fact that neurons in **L**VI are the exclusive origin of entorhinal thalamic projections [51]. The fact that the dendrites and axons of **L**VI principal neurons can pass the border to the pre- and parasubiculum suggests that they might contribute to inter-area communication between the hippocampus, subiculum and the pre- and parasubiculum. The axonal distribution makes it likely that **L**VI principal neurons can communicate with neurons in **L**III-**L**VI [57].

2. Lack of correlation between morphology and physiology, except for layer II

With the exception of principal neurons in **L**II, we did not observe a clear correlation between the morphology and physiology of individual principal neurons. Principal neurons in **L**V show diverse firing patterns not clearly related to any morphological neuron type [22]. Principal neurons in **L**III and **L**VI of MEC have very homogenous firing patterns and a correlation to a specific morphology is thus not apparent. The questions that remain to be answered are whether neurons with a common *in vitro* physiological but different morphological profile are functionally different *in vivo* [9] and if so how the *in vitro* and *in vivo* characteristics can be equated.

Within **L**II, all morphological SCs had a SC physiology. Among pyramidal neurons the majority had a pyramidal-like physiology, that is different from SCs, but some had a sag potential and rebound amplitude, i.e. features of SCs. This is in line with earlier findings [21]. Our data can be best interpreted as pointing to the presence of two, physiologically and morphologically defined, principal neuron types in **L**II with several types in between. This suggests that at least two functionally different cell types may exist *in vivo* in **L**II of MEC. This may correspond to a recent description of two types, one that projects outside the hippocampus and can induce depolarization-induced suppression of inhibition (DSI), and another that projects to the hippocampus and cannot induce DSI [58]. Whether only one of these two main cell types represent the grid cells with the other representing another cell type, remains to be established.

For MEC **L**III it has been shown that extrinsic stimulation enables to differentiate between cell types [19, 50] suggesting that differences in inputs play

a relevant role in establishing differences in *in vivo* properties [9], by interacting with individual neuronal properties. The latter in turn may depend on the local circuitry.
The identification of neurochemical specificity or the genetic fingerprint of neurons in all layers, as well as neural response specificity in the intact network to modulators such as acetylcholine or dopamine, will likely contribute to the understanding of how physiological differentiation occurs within a layer or in the overall network [25, 59-63].

3. Layer specific physiological properties and functional relevance

Layer I and layer II. **L**I and **L**II principal neurons have several characteristics that differ from principal neurons in all other layers. A lower input resistance and shorter time constant makes them less excitable. In addition we found that the majority has a prominent sag potential in the hyperpolarizing and depolarizing direction [17], not observed in any of the other layers. The sag potential in the depolarizing direction leads to non-delayed firing in response to extrinsic excitation. It has been shown that the h-current in conjunction with other voltage dependent currents, is responsible for membrane oscillations in **L**II [64, 65]. Membrane oscillations, which are in the theta range in **L**II, have been suggested to be instrumental in the formation of grid cells and phase precession in MEC [13, 14], and to act as a frequency dependent amplifier of small-amplitude signals [64, 66, 67]. The latter suggests that these features may be instrumental to gate the pathway from **L**II to the dentate gyrus in a theta frequency-dependent manner [67-69], which is less prominent in LEC [1, 70].
In accordance with previous accounts we found that the rebound amplitude induced after hyperpolarization of **L**II principal neurons leads to excitation after the offset of hyperpolarizing current steps, which can lead to firing [17, 21]. *In vivo* a rebound might induce immediate depolarization after strong inhibition. The stronger the preceding inhibition, the bigger the rebound amplitude. The rebound potential, which has been shown to persist in the presence of Cs^+ [71] and after TTX application [21], is suggested to be induced by a low voltage activated Ca^{2+} current [21]. Specific Ca^{2+} regulation in MEC **L**II might also explain the existence of DAPs, unique for **L**II neurons [21]. DAPs can induce bursting activity and have been suggested to play a role in phase precession and persistent firing *in vivo* [72-74], although in other entorhinal layers as well as in other cortical areas persistent firing of neurons not showing DAPs has been reported [75, 76].

Layer III. Our data corroborate previously published ones that **L**III principal neurons in general do not have a prominent sag potential in either direction, no DAPs, no resonance and membrane potential oscillations [18, 21, 50]. That **L**III principal neurons lack a sag potential is likely caused by a lack in activated h-

channels [77]. The absence of a sag potential in the depolarizing direction can be the cause of the observed delayed firing. The absence of firing in bursts might be related to the fact the **L**III principal neurons do not have DAPs. This feature as well as the presence of SFA in response to strong depolarization may results from a difference in Ca^{2+} regulation in **L**III compared to **L**II and **L**VI principal neurons [21]. MEC and LEC neurons do not differ significantly with respect to the input resistance, time constant, sag ratio, rebound and DAP amplitudes, as well as the AP rise time and width.

Layer V. The most striking observation is the heterogeneity among **L**V principal neurons, in particular with respect to DAPs after the first AP, sag potentials in the hyperpolarizing direction and the degree of SFA [22]. These differences in properties may relate to the observed diversity in *in vivo* firing patterns e.g. some neurons show phase precession some not [72]. Further, we found that most **L**V principal neurons do not have prominent membrane oscillations and that, if present, the membrane oscillates at high frequency (between 10.9 and 18.16 Hz). These observations are in contrast to two reports that showed that at least two-third of principal neurons in MEC **L**V have oscillations with a frequency ranging from 3 - 30 Hz [78] or 3.4 - 14.8 Hz [22]. Differences in data might be due the fact that we patched in P14 to P32 old rats instead of 150 - 250 g rats, i.e. P60 animals, used in the previous studies and that age dependent changes occur [79]. It is thus likely that the network integration in **L**V of younger animals is less frequency dependent than in older animals [54, 66, 72].
We found that in most principal neurons the amplitudes of the APs in a spike train decrease significantly, sometimes resulting in the cessation of spiking within an ongoing stimulus. Additionally, principal neurons show prominent SFA. This suggests that **L**V principal neurons are particularly responsive to repetitive short stimulation. Adding carbachol to the slice or an increased activity of the basal forebrain output *in vivo* can augment SFA and the decrease in AP amplitude, leading to persistent firing [25, 80, 81]. Thereby **L**V neurons can change to a different state under certain conditions, such as attention. Since MEC and LEC **L**V principal neurons do not show prominent differences, this is likely to hold true for LEC [1].

Layer VI. Principal neurons in **L**VI do not have a prominent sag potential in either depolarizing or hyperpolarizing direction, no DAPs, no resonance and no membrane potential oscillations and are in that respect similar to principal neurons in **L**III as well as to their counterparts in **L**VI of LEC. These physiological characteristics, combined with the specific morphology, strongly separate **L**VI principal neurons functionally from **L**V principal neurons. Their dissociation from **L**V principal neurons as well as their homogeneity across the

two entorhinal subdivisions is supported by observations that neurons in both MEC and LEC share a response to nicotinic activation, which is unique and not seen in other layers of either entorhinal domain [57]. The observed differences in input resistance and time constant between MEC and LEC indicate that MEC principal neurons are likely to be less excitable compared to LEC **L**VI principal neurons.

Main determinants of *in vivo* properties of neurons and networks.

Principal neurons within MEC show clear layer specific morphological and physiological properties, which likely bear to the fact that neurons in different layers show different *in vivo* functional properties [8-10]. The most profound differences are between principal neurons in **L**II and those in **L**III-**L**VI, which may correspond to the striking observation that a large percentage of **L**II are grid cells, which are less frequently found in other layers [9]. However, within **L**III-**L**VI, principal neurons still differ from each other, which raises the intriguing question how this relates to recent reports that principal neurons in **L**III-**L**VI show strikingly similar *in vivo* spatial firing properties [9, 82]. Since it is unlikely that these layers share overall intrinsic organizational principles that produce such commonality, we propose that a common input imposed on the layer specific networks is the more parsimonious explanation. In light of the recent finding that neurons with strikingly similar *in vivo* properties exist in the pre- and parasubiculum [82], which both are major input structures to MEC [83, 84], it is tempting to suggest that these inputs play a relevant role. We have recently shown that principal neurons in all layers of MEC are targeted monosynaptically by both inputs, which strengthens this notion [55]. Laminar differences in integrative properties [55], likely are the result of the here reported layer specific cellular properties.

Besides input from head direction cells, differences in *in vitro* biophysical membrane properties, have been implicated as relevant factors in grid cell formation in MEC **L**II [11-15, 85]. Here we reported that electrophysiological properties of **L**II principal neurons change along the mediolateral axis in MEC, continuing across the lateral MEC border into LEC. Comparable observations were made when comparing SCs in **L**II of MEC along the dorsoventral axis [12, 15]. If these properties influence the frequency, scale and specificity of grid cell firing as has been suggested [15], these findings together would thus indicate that the slope of gradual changes in frequency, scale, and specificity will be steepest when comparing dorsomedial neurons to more ventrolaterally positioned ones.

Our data indicate that the anatomical border between MEC and LEC does not coincide with a clear physiological border in **L**II for the properties tested. This lack of a clear border in **L**II is supported by the observation that principal neurons in **L**II at the border between MEC and LEC have axons and dendrites

that cross the border. Both, the physiological and morphological observations, may correlate with the concept of entorhinal bands defined on the basis of topographically organized hippocampal connections [30-33] and intrinsic connections [34]. If true, this would suggest that functionally similar neurons are to be found in portions of LEC that are close to the border with MEC, particularly at dorsal levels. This has not been tested although it is well established that grid cells or spatially modulated neurons are not present in ventrolaterally positioned **L**II neurons in LEC [28].

3.4 References

1. Canto, C.B. & Witter, M.P. Cellular properties of principal neurons in the rat entorhinal cortex. I. The lateral entorhinal cortex. *Hippocampus* **Submitted** (2011).
2. Eichenbaum, H. & Lipton, P.A. Towards a functional organization of the medial temporal lobe memory system: role of the parahippocampal and medial entorhinal cortical areas. *Hippocampus* **18**, 1314-1324 (2008).
3. Brun, V.H.*, et al.* Impaired spatial representation in CA1 after lesion of direct input from entorhinal cortex. *Neuron* **57**, 290-302 (2008).
4. Van Cauter, T., Poucet, B. & Save, E. Unstable CA1 place cell representation in rats with entorhinal cortex lesions. *Eur. J. Neurosci.* **27**, 1933-1946 (2008).
5. Dickerson, B.C. & Eichenbaum, H. The episodic memory system: neurocircuitry and disorders. *Neuropsychopharmacology* **35**, 86-104 (2010).
6. Steffenach, H.A., Witter, M., Moser, M.B. & Moser, E.I. Spatial memory in the rat requires the dorsolateral band of the entorhinal cortex. *Neuron* **45**, 301-313 (2005).
7. Fyhn, M., Molden, S., Witter, M.P., Moser, E.I. & Moser, M.B. Spatial representation in the entorhinal cortex. *Science* **305**, 1258-1264 (2004).
8. Hafting, T., Fyhn, M., Molden, S., Moser, M.B. & Moser, E.I. Microstructure of a spatial map in the entorhinal cortex. *Nature* **436**, 801-806 (2005).
9. Sargolini, F.*, et al.* Conjunctive representation of position, direction, and velocity in entorhinal cortex. *Science* **312**, 758-762 (2006).
10. Solstad, T., Boccara, C.N., Kropff, E., Moser, M.B. & Moser, E.I. Representation of geometric borders in the entorhinal cortex. *Science* **322**, 1865-1868 (2008).
11. McNaughton, B.L., Battaglia, F.P., Jensen, O., Moser, E.I. & Moser, M.B. Path integration and the neural basis of the 'cognitive map'. *Nat. Rev. Neurosci.* **7**, 663-678 (2006).
12. Garden, D.L., Dodson, P.D., O'Donnell, C., White, M.D. & Nolan, M.F. Tuning of synaptic integration in the medial entorhinal cortex to the organization of grid cell firing fields. *Neuron* **60**, 875-889 (2008).
13. Hasselmo, M.E., Giocomo, L.M. & Zilli, E.A. Grid cell firing may arise from interference of theta frequency membrane potential oscillations in single neurons. *Hippocampus* **17**, 1252-1271 (2007).
14. Burgess, N., Barry, C. & O'Keefe, J. An oscillatory interference model of grid cell firing. *Hippocampus* **17**, 801-812 (2007).

15. Giocomo, L.M., Zilli, E.A., Fransen, E. & Hasselmo, M.E. Temporal frequency of subthreshold oscillations scales with entorhinal grid cell field spacing. *Science* **315**, 1719-1722 (2007).

16. Klink, R. & Alonso, A. Morphological characteristics of layer II projection neurons in the rat medial entorhinal cortex. *Hippocampus* **7**, 571-583 (1997).

17. Alonso, A. & Klink, R. Differential electroresponsiveness of stellate and pyramidal-like cells of medial entorhinal cortex layer II. *J. Neurophysiol.* **70**, 128-143 (1993).

18. Dickson, C.T., Mena, A.R. & Alonso, A. Electroresponsiveness of medial entorhinal cortex layer III neurons in vitro. *Neuroscience* **81**, 937-950 (1997).

19. Gloveli, T., Schmitz, D. & Heinemann, U. Prolonged inhibitory potentials in layer III projection cells of the rat medial entorhinal cortex induced by synaptic stimulation in vitro. *Neuroscience* **80**, 119-131 (1997).

20. Gloveli, T., Dugladze, T., Schmitz, D. & Heinemann, U. Properties of entorhinal cortex deep layer neurons projecting to the rat dentate gyrus. *Eur. J. Neurosci.* **13**, 413-420 (2001).

21. Van der Linden, S. & Lopes da Silva, F.H. Comparison of the electrophysiology and morphology of layers III and II neurons of the rat medial entorhinal cortex in vitro. *Eur. J. Neurosci.* **10**, 1479-1489 (1998).

22. Hamam, B.N., Kennedy, T.E., Alonso, A. & Amaral, D.G. Morphological and electrophysiological characteristics of layer V neurons of the rat medial entorhinal cortex. *J. Comp. Neurol.* **418**, 457-472 (2000).

23. Lingenhohl, K. & Finch, D.M. Morphological characterization of rat entorhinal neurons in vivo: soma-dendritic structure and axonal domains. *Exp. Brain Res.* **84**, 57-74 (1991).

24. Fransen, E., Tahvildari, B., Egorov, A.V., Hasselmo, M.E. & Alonso, A.A. Mechanism of graded persistent cellular activity of entorhinal cortex layer v neurons. *Neuron* **49**, 735-746 (2006).

25. Egorov, A.V., Hamam, B.N., Fransen, E., Hasselmo, M.E. & Alonso, A.A. Graded persistent activity in entorhinal cortex neurons. *Nature* **420**, 173-178 (2002).

26. Langston, R.F.*, et al.* Development of the spatial representation system in the rat. *Science* **328**, 1576-1580 (2010).

27. Wills, T.J., Cacucci, F., Burgess, N. & O'Keefe, J. Development of the hippocampal cognitive map in preweanling rats. *Science* **328**, 1573-1576 (2010).

28. Hargreaves, E.L., Rao, G., Lee, I. & Knierim, J.J. Major dissociation between medial and lateral entorhinal input to dorsal hippocampus. *Science* **308**, 1792-1794 (2005).

29. Knierim, J.J. Neural representations of location outside the hippocampus. *Learn. Mem.* **13**, 405-415 (2006).

30. Dolorfo, C.L. & Amaral, D.G. Entorhinal cortex of the rat: topographic organization of the cells of origin of the perforant path projection to the dentate gyrus. *J. Comp Neurol.* **398**, 25-48 (1998).

31. Witter, M.P., van Hoesen, G.W. & Amaral, D.G. Topographical organization of the entorhinal projection to the dentate gyrus of the monkey. *J. Neurosci.* **9**, 216-228 (1989).

32. Kloosterman, F., van Haeften, T. & Lopes da Silva, F.H. Two reentrant pathways in the hippocampal-entorhinal system. *Hippocampus* **14**, 1026-1039 (2004).

33. Tamamaki, N. & Nojyo, Y. Projection of the entorhinal layer II neurons in the rat as revealed by intracellular pressure-injection of neurobiotin. *Hippocampus* **3**, 471-480 (1993).

34. Dolorfo, C.L. & Amaral, D.G. Entorhinal cortex of the rat: organization of intrinsic connections. *J. Comp. Neurol.* **398**, 49-82 (1998).

35. McCormick, D.A., Connors, B.W., Lighthall, J.W. & Prince, D.A. Comparative electrophysiology of pyramidal and sparsely spiny stellate neurons of the neocortex. *J. Neurophysiol.* **54**, 782-806 (1985).

36. Rudy, B. & McBain, C.J. Kv3 channels: voltage-gated K+ channels designed for high-frequency repetitive firing. *Trends Neurosci.* **24**, 517-526 (2001).

37. Jones, R.S. & Buhl, E.H. Basket-like interneurones in layer II of the entorhinal cortex exhibit a powerful NMDA-mediated synaptic excitation. *Neurosci. Lett.* **149**, 35-39 (1993).

38. Brun, V.H.*, et al.* Progressive increase in grid scale from dorsal to ventral medial entorhinal cortex. *Hippocampus* **18**, 1200-1212 (2008).

39. Lorente de Nó, R. Studies on the structure of the cerebral cortex. *Journal fur Psychologie und Neurologie* **45**, 381-438 (1933).

40. Miettinen, M., Pitkanen, A. & Miettinen, R. Distribution of calretinin-immunoreactivity in the rat entorhinal cortex: coexistence with GABA. *J. Comp. Neurol.* **378**, 363-378 (1997).

41. Wouterlood, F.G., van Denderen, J.C., van Haeften, T. & Witter, M.P. Calretinin in the entorhinal cortex of the rat: distribution, morphology, ultrastructure of neurons, and co-localization with gamma-aminobutyric acid and parvalbumin. *J. Comp. Neurol.* **425**, 177-192 (2000).

42. Germroth, P., Schwerdtfeger, W.K. & Buhl, E.H. GABAergic neurons in the entorhinal cortex project to the hippocampus. *Brain Res.* **494**, 187-192 (1989).

43. Wouterlood, F.G. & Pothuizen, H. Sparse colocalization of somatostatin- and GABA-immunoreactivity in the entorhinal cortex of the rat. *Hippocampus* **10**, 77-86 (2000).

44. Gatome, C.W., Slomianka, L., Lipp, H.P. & Amrein, I. Number estimates of neuronal phenotypes in layer II of the medial entorhinal cortex of rat and mouse. *Neuroscience* **170**, 156-165 (2010).

45. Jones, R.S. Synaptic and intrinsic properties of neurons of origin of the perforant path in layer II of the rat entorhinal cortex in vitro. *Hippocampus* **4**, 335-353 (1994).

46. Tahvildari, B. & Alonso, A. Morphological and electrophysiological properties of lateral entorhinal cortex layers II and III principal neurons. *J. Comp. Neurol.* **491**, 123-140 (2005).

47. Quilichini, P., Sirota, A. & Buzsaki, G. Intrinsic circuit organization and theta-gamma oscillation dynamics in the entorhinal cortex of the rat. *J. Neurosci.* **30**, 11128-11142 (2010).

48. Dhillon, A. & Jones, R.S. Laminar differences in recurrent excitatory transmission in the rat entorhinal cortex in vitro. *Neuroscience* **99**, 413-422 (2000).

49. Kumar, S.S., Jin, X., Buckmaster, P.S. & Huguenard, J.R. Recurrent circuits in layer II of medial entorhinal cortex in a model of temporal lobe epilepsy. *J. Neurosci.* **27**, 1239-1246 (2007).

50. Gloveli, T., Schmitz, D., Empson, R.M., Dugladze, T. & Heinemann, U. Morphological and electrophysiological characterization of layer III cells of the medial entorhinal cortex of the rat. *Neuroscience* **77**, 629-648 (1997).

51. Witter, M.P. & Amaral, D.G. Hippocampal formation. in *The Rat Nervous System.* (ed. G. Paxinos) 635-704 (Academic Press, San Diego, Calif., USA, 2004).

52. Beed, P*., et al.* Analysis of excitatory microcircuitry in the medial entorhinal cortex reveals cell-type-specific differences. *Neuron* **68**, 1059-1066 (2010).

53. Ramon y Cajal, S. Sobre un ganglio especial de la corteza esfenooccipital. *Trab Lab Invest Biol Univ Madrid* **1**, 189-201 (1902).

54. Hamam, B.N., Amaral, D.G. & Alonso, A.A. Morphological and electrophysiological characteristics of layer V neurons of the rat lateral entorhinal cortex. *J. Comp. Neurol.* **451**, 45-61 (2002).

55. Canto, C.B., Koganezawa, N., Beed, P. & Witter, M.P. Monosynaptic Inputs from Presubiculum and Parasubiculum Converge on Medial Entorhinal Cortex Principal Neurons *To be subm*itted to *Nat. Neurosci.* **To be Submitted** (2011).

56. Canto, C.B. & Witter, M.P. Inputs from Presubiculum and Parasubiculum Converge on Medial Entorhinal Cortex Principal Neurons in *Federation of European Neuroscience* (Amsterdam, 2010).

57. Tu, B., Gu, Z., Shen, J.X., Lamb, P.W. & Yakel, J.L. Characterization of a nicotine-sensitive neuronal population in rat entorhinal cortex. *J. Neurosci.* **29**, 10436-10448 (2009).

58. Varga, C., Lee, S.Y. & Soltesz, I. Target-selective GABAergic control of entorhinal cortex output. *Nat. Neurosci.* **13**, 822-824 (2010).

59. Klausberger, T., Roberts, J.D. & Somogyi, P. Cell type- and input-specific differences in the number and subtypes of synaptic GABA(A) receptors in the hippocampus. *J. Neurosci.* **22**, 2513-2521 (2002).

60. Klausberger, T. & Somogyi, P. Neuronal diversity and temporal dynamics: the unity of hippocampal circuit operations. *Science* **321**, 53-57 (2008).

61. Somogyi, P. & Klausberger, T. Defined types of cortical interneurone structure space and spike timing in the hippocampus. *J. Physiol.* **562**, 9-26 (2005).

62. Tahvildari, B., Alonso, A.A. & Bourque, C.W. Ionic basis of ON and OFF persistent activity in layer III lateral entorhinal cortical principal neurons. *J. Neurophysiol.* **99**, 2006-2011 (2008).

63. Heys, J.G., Giocomo, L.M. & Hasselmo, M.E. Cholinergic modulation of the resonance properties of stellate cells in layer II of medial entorhinal cortex. *J. Neurophysiol.* **104**, 258-270 (2010).

64. Dickson, C.T.*, et al.* Properties and role of I(h) in the pacing of subthreshold oscillations in entorhinal cortex layer II neurons. *J. Neurophysiol.* **83**, 2562-2579 (2000).

65. Giocomo, L.M. & Hasselmo, M.E. Knock-out of HCN1 subunit flattens dorsal-ventral frequency gradient of medial entorhinal neurons in adult mice. *J. Neurosci.* **29**, 7625-7630 (2009).

66. Hutcheon, B., Miura, R.M. & Puil, E. Subthreshold membrane resonance in neocortical neurons. *J. Neurophysiol.* **76**, 683-697 (1996).

67. Erchova, I., Kreck, G., Heinemann, U. & Herz, A.V. Dynamics of rat entorhinal cortex layer II and III cells: characteristics of membrane potential resonance at rest predict oscillation properties near threshold. *J. Physiol.* **560**, 89-110 (2004).

68. Gloveli, T., Schmitz, D., Empson, R.M. & Heinemann, U. Frequency-dependent information flow from the entorhinal cortex to the hippocampus. *J. Neurophysiol.* **78**, 3444-3449 (1997).

69. Schreiber, S., Erchova, I., Heinemann, U. & Herz, A.V. Subthreshold resonance explains the frequency-dependent integration of periodic as well as random stimuli in the entorhinal cortex. *J. Neurophysiol.* **92**, 408-415 (2004).

70. Deshmukh, S.S., Yoganarasimha, D., Voicu, H. & Knierim, J.J. Theta modulation in the medial and the lateral entorhinal cortices. *J. Neurophysiol.* **104**, 994-1006 (2010).

71. Klink, R. & Alonso, A. Ionic mechanisms for the subthreshold oscillations and differential electroresponsiveness of medial entorhinal cortex layer II neurons. *J. Neurophysiol.* **70**, 144-157 (1993).

72. Hafting, T., Fyhn, M., Bonnevie, T., Moser, M.B. & Moser, E.I. Hippocampus-independent phase precession in entorhinal grid cells. *Nature* **453**, 1248-1252 (2008).

73. Lisman, J.E., Talamini, L.M. & Raffone, A. Recall of memory sequences by interaction of the dentate and CA3: a revised model of the phase precession. *Neural Netw.* **18**, 1191-1201 (2005).

74. Koene, R.A. & Hasselmo, M.E. First-in-first-out item replacement in a model of short-term memory based on persistent spiking. *Cereb. Cortex* **17**, 1766-1781 (2007).

75. Tahvildari, B., Fransen, E., Alonso, A.A. & Hasselmo, M.E. Switching between "On" and "Off" states of persistent activity in lateral entorhinal layer III neurons. *Hippocampus* **17**, 257-263 (2007).

76. Woodward, J.J. & Pava, M.J. Effects of ethanol on persistent activity and up-States in excitatory and inhibitory neurons in prefrontal cortex. *Alcohol. Clin. Exp. Res.* **33**, 2134-2140 (2009).

77. Shah, M.M., Anderson, A.E., Leung, V., Lin, X. & Johnston, D. Seizure-induced plasticity of h channels in entorhinal cortical layer III pyramidal neurons. *Neuron* **44**, 495-508 (2004).

78. Schmitz, D., Gloveli, T., Behr, J., Dugladze, T. & Heinemann, U. Subthreshold membrane potential oscillations in neurons of deep layers of the entorhinal cortex. *Neuroscience* **85**, 999-1004 (1998).

79. Reboreda, A., Raouf, R., Alonso, A. & Seguela, P. Development of cholinergic modulation and graded persistent activity in layer v of medial entorhinal cortex. *J. Neurophysiol.* **97**, 3937-3947 (2007).

80. Alonso, A. & Kohler, C. A study of the reciprocal connections between the septum and the entorhinal area using anterograde and retrograde axonal transport methods in the rat brain. *J. Comp. Neurol.* **225**, 327-343 (1984).

81. Milner, T.A., Loy, R. & Amaral, D.G. An anatomical study of the development of the septo-hippocampal projection in the rat. *Brain Res.* **284**, 343-371 (1983).

82. Boccara, C.N.*, et al.* Grid cells in pre- and parasubiculum. *Nat. Neurosci.* **13**, 987-994 (2010).

83. Caballero-Bleda, M. & Witter, M.P. Regional and laminar organization of projections from the presubiculum and parasubiculum to the entorhinal cortex: an anterograde tracing study in the rat. *J. Comp. Neurol.* **328**, 115-129 (1993).

84. Kerr, K.M., Agster, K.L., Furtak, S.C. & Burwell, R.D. Functional neuroanatomy of the parahippocampal region: the lateral and medial entorhinal areas. *Hippocampus* **17**, 697-708 (2007).

85. Moser, E.I., Kropff, E. & Moser, M.B. Place cells, grid cells, and the brain's spatial representation system. *Annu. Rev. Neurosci.* **31**, 69-89 (2008).

3

3